# The SUN protein Mps3 controls Ndc1 distribution and function on the nuclear membrane

Jingjing Chen,[1] Christine J. Smoyer,[1] Brian D. Slaughter,[1] Jay R. Unruh,[1] and Sue L. Jaspersen[1,2]

[1]Stowers Institute for Medical Research, Kansas City, MO 64110
[2]Department of Molecular and Integrative Physiology, University of Kansas Medical Center, Kansas City, KS 66160

In closed mitotic systems such as *Saccharomyces cerevisiae*, nuclear pore complexes (NPCs) and the spindle pole body (SPB) must assemble into an intact nuclear envelope (NE). Ndc1 is a highly conserved integral membrane protein involved in insertion of both complexes. In this study, we show that Ndc1 interacts with the SUN domain–containing protein Mps3 on the NE in live yeast cells using fluorescence cross-correlation spectroscopy. Genetic and molecular analysis of a series of new *ndc1* alleles allowed us to understand the role of Ndc1–Mps3 binding at the NE. We show that the *ndc1-L562S* allele is unable to associate specifically with Mps3 and find that this mutant is lethal due to a defect in SPB duplication. Unlike other *ndc1* alleles, the growth and Mps3 binding defect of *ndc1-L562S* is fully suppressed by deletion of *POM152*, which encodes a NPC component. Based on our data we propose that the Ndc1–Mps3 interaction is important for controlling the distribution of Ndc1 between the NPC and SPB.

## Introduction

Separation of cytoplasm and nucleoplasm in eukaryotic cells is achieved by formation of the nuclear envelope (NE), which is a double lipid bilayer composed of an outer nuclear membrane (ONM) that is contiguous with the endoplasmic reticulum (ER) and an inner nuclear membrane (INM) that contains a distinct set of proteins from either the ONM or the ER. Bidirectional transport of molecules across the NE occurs through nuclear pore complexes (NPCs) that are embedded in the nuclear membrane at sites where the INM and ONM are contiguous, forming a pore membrane (POM; Strambio-De-Castillia et al., 2010; Aitchison and Rout, 2012). In metazoans, two pathways exist for NPC formation: a mitotic pathway in which NPC assembly is coupled with reformation of the NE in telophase, and a de novo assembly pathway in which NPCs are inserted into an intact NE during interphase. In fungi that undergo a closed mitosis in which the NE remains intact, NPC assembly occurs exclusively through the de novo pathway (Hetzer and Wente, 2009; Aitchison and Rout, 2012).

During mitosis, the NE poses a challenge in terms of formation of the mitotic spindle because components of the chromosome segregation machinery, such as the microtubule organizing center (MTOC, known as the centrosome in metazoans and the spindle pole body [SPB] in fungi), are located in the cytoplasm whereas the DNA is located inside the nucleus. Multiple strategies have evolved for overcoming this obstacle, including disassembly of the NE, which occurs in prometaphase in most metazoans, or incorporation of the SPB into the NE, which occurs in fungi. In budding yeast, the SPB is present in the NE throughout the lifecycle (Byers and Goetsch, 1975). Like the NPC, the INM and ONM appear to form a contiguous pore membrane at the SPB (O'Toole et al., 1999). In contrast, the fission yeast SPB is only transiently inserted into the NE during mitosis (McCully and Robinow, 1971; Ding et al., 1997). During interphase, the *Schizosaccharomyces pombe* SPB resides in a NE invagination similar to that seen in some types of vertebrate cells, raising the interesting possibility that a physical linkage may tether MTOCs to the NE throughout cell division (Robbins and Gonatas, 1964; Stafstrom and Staehelin, 1984; Baker et al., 1993; Tang and Marshall, 2012). One class of MTOC anchor to the NE is the conserved SUN (for Sad1–UNC-84

Correspondence to Sue L. Jaspersen: slj@stowers.org

Abbreviations used in this paper: 3-AT, 3-aminotriazole; 5-FOA, 5-fluoroorotic acid; ALPS, Arf1GAP lipid-packing sensor; Cub, C terminus of ubiquitin; FCCS, fluorescence cross-correlation spectroscopy; FRET, fluorescence resonance energy transfer; INM, inner nuclear membrane; MTOC, microtubule-organizing center; MYTH, membrane-based yeast two hybrid; NE, nuclear envelope; NPC, nuclear pore complex; Nub, N terminus of ubiquitin; ONM, outer nuclear membrane; POM, pore membrane; SPB, spindle pole body; SUN, Sad1–UNC-84 homology; ts, temperature sensitive.



The Rockefeller University Press $30.00
J. Cell Biol. Vol. 204 No. 4 523–539
www.jcb.org/cgi/doi/10.1083/jcb.201307043

homology) family of INM proteins (Starr and Fridolfsson, 2010; Rothballer and Kutay, 2013).

Cytological analysis of SPB duplication in *Saccharomyces cerevisiae* and NPC assembly in *Xenopus* extracts has revealed several common assembly principles that are important for NE insertion of both complexes, including the step-wise assembly of each complex and the requirement for formation of the pore membrane (Byers and Goetsch, 1974, 1975; Goldberg et al., 1997). Further characterization of NPC assembly points to a role for ER membrane–shaping proteins such as the reticulons and Yop1/DP1 in generation of membrane curvature (Dawson et al., 2009). It is thought that additional membrane remodeling events such as changes in lipid composition and stabilization of the highly curved pore membrane by certain classes of proteins, including the ALPS proteins (for Afr1GAP lipid-packing sensor) also occur (Bigay et al., 2005; Hetzer and Wente, 2009; Rothballer and Kutay, 2013). Much less is known about the mechanism of SPB insertion into the NE, although recent work points to a role for Rtn1 and Yop1 in SPB assembly, and at least one SPB component, Nbp1, contains an ALPS domain (Kupke et al., 2011; Casey et al., 2012).

A key player in NE insertion of both NPCs and SPBs is the conserved integral membrane protein Ndc1 (known as Cut11 in fission yeast; Chial et al., 1998; West et al., 1998; Araki et al., 2006). As the only known component that is shared between the SPB and NPC, knowledge of Ndc1 regulation, distribution, and function is critical to understanding how NE processes are controlled. Analysis of Ndc1 secondary structure shows that the N-terminal half contains six transmembrane domains. The C terminus is thought to form a surface for interaction with proteins, including Nbp1 at the SPB and Pom34 and Pom152 at the NPC (Araki et al., 2006; Lau et al., 2006; Onischenko et al., 2009). Through its interactions with these and other proteins, including reticulons and Yop1, Ndc1 most likely plays a role in formation of the pore membrane at both the NPC and SPB (Araki et al., 2006; Madrid et al., 2006; Onischenko et al., 2009; Casey et al., 2012). Although vertebrates do not contain MTOCs embedded in their NE, it is interesting to note that Ndc1 has been identified in some MTOC preparations such as ciliary pore complexes (Ounjai et al., 2013). Additionally, the region of the NE surrounding the centrosome is first to disassemble during early mitosis in *Caenorhabditis elegans* embryos, suggesting that centrosome-associated factors may trigger NE remodeling (Hachet et al., 2012; Ounjai et al., 2013). Ndc1 is also present at NPCs in higher eukaryotes, interacting with Pom121, Nup210/gp210, and other nucleoporins during both postmitotic and de novo NPC assembly (Mansfeld et al., 2006; Stavru et al., 2006; Rasala et al., 2008; Mitchell et al., 2010).

To understand the role that Ndc1 plays in duplication and insertion of NPCs and SPBs, we analyzed mutants in conserved residues in Ndc1 for their ability to interact with known NPC and SPB components and to function as the sole copy of *NDC1* in budding yeast. Three classes of mutants were identified, including (1) lethal alleles that are unable to interact with SPB or NPC components such as *ndc1-V180G*; (2) conditional alleles that are able to interact with NPC components but not with SPB components, resulting in defects in SPB duplication such as *ndc1-A290E*; and (3) lethal alleles that are able to interact with known SPB and NPC components such as *ndc1-L562S*. Characterization of *ndc1-L562S* showed that lethality is due to a defect in SPB duplication, and the growth defect of this mutant, but not other classes of alleles, could be fully rescued by *pom152Δ*. Deletion of *POM152* resulted in increased levels of ndc1-L562S, but no change in binding to Nbp1 or Pom34 was observed, suggesting that Ndc1 has an additional binding partner that is important for SPB duplication. Multiple lines of evidence indicate that the SUN protein Mps3 binds to Ndc1 at the NE and partitions it between the NPC and SPB.

## Results

### An assay for Ndc1 binding at the NPC and SPB

To study the recruitment of Ndc1 to the SPB and NPC, we set up a membrane-based yeast two-hybrid (MYTH) system (Fig. 1 A; Stagljar and Fields, 2002; Thaminy et al., 2003; Snider et al., 2010). The bait, *NDC1* (or mutant derivatives), was fused with the C terminus of ubiquitin (Cub) and expressed using the *CYC1* promoter on a low-copy *LEU2*-marked centromeric plasmid. This resulted in low levels of Ndc1 expression at the NE compared with Ndc1 expressed from the chromosomal locus or a *GAL1*-driven version of *NDC1-GFP* (Fig. 1, B and C). The preys were fused with a mutant version of the N terminus of ubiquitin (NubG) that cannot associate with the C-terminal ubiquitin domain and expressed using the *ADH1* promoter on a *TRP1*-marked plasmid.

To examine recruitment of Ndc1 to the NPC and SPB, we used Pom152 and Pom34 as our NPC preys because they form a well-established NPC subcomplex of the NPC with Ndc1 (Madrid et al., 2006; Alber et al., 2007; Onischenko et al., 2009). Nbp1 is the only known Ndc1 binding partner at the SPB, so it was our SPB prey (Araki et al., 2006). If the bait and prey proteins associate, a transcription factor (LexA-VP16) that is part of the Ndc1 bait construct is cleaved, and the soluble transcription factor stimulates expression of the reporter genes *HIS3* and *ADE2*, which allows growth on media lacking histidine and adenine. Because mutations in *ade2* result in accumulation of a red pigment, colony color can be used as a qualitative measure of binding: red, pink, and white for no, weak, and strong interactions, respectively. As shown in Fig. 1 D, Ndc1 is able to strongly interact with Nbp1, Pom152, and Pom34 in the MYTH system.

Analysis of ndc1-39 showed that it was able to bind to Pom152 and Pom34, but very weakly interacted with Npb1 in our MYTH assay at 30°C (Fig. 1 E; Fig. S2 A). The failure of ndc1-39 to bind to Nbp1 has been observed previously using a GAL4-based version of the yeast two-hybrid system (Araki et al., 2006). However, because we were unable to detect binding between Ndc1 and either Pom152 or Pom34 in the GAL4-based system (unpublished data), we used the MYTH system for our studies of Ndc1-interacting proteins. The SPB duplication defect in *ndc1-39* is thought to arise due to the Nbp1 binding defect, demonstrating utility of the MYTH system for isolating and characterizing new *NDC1* alleles.

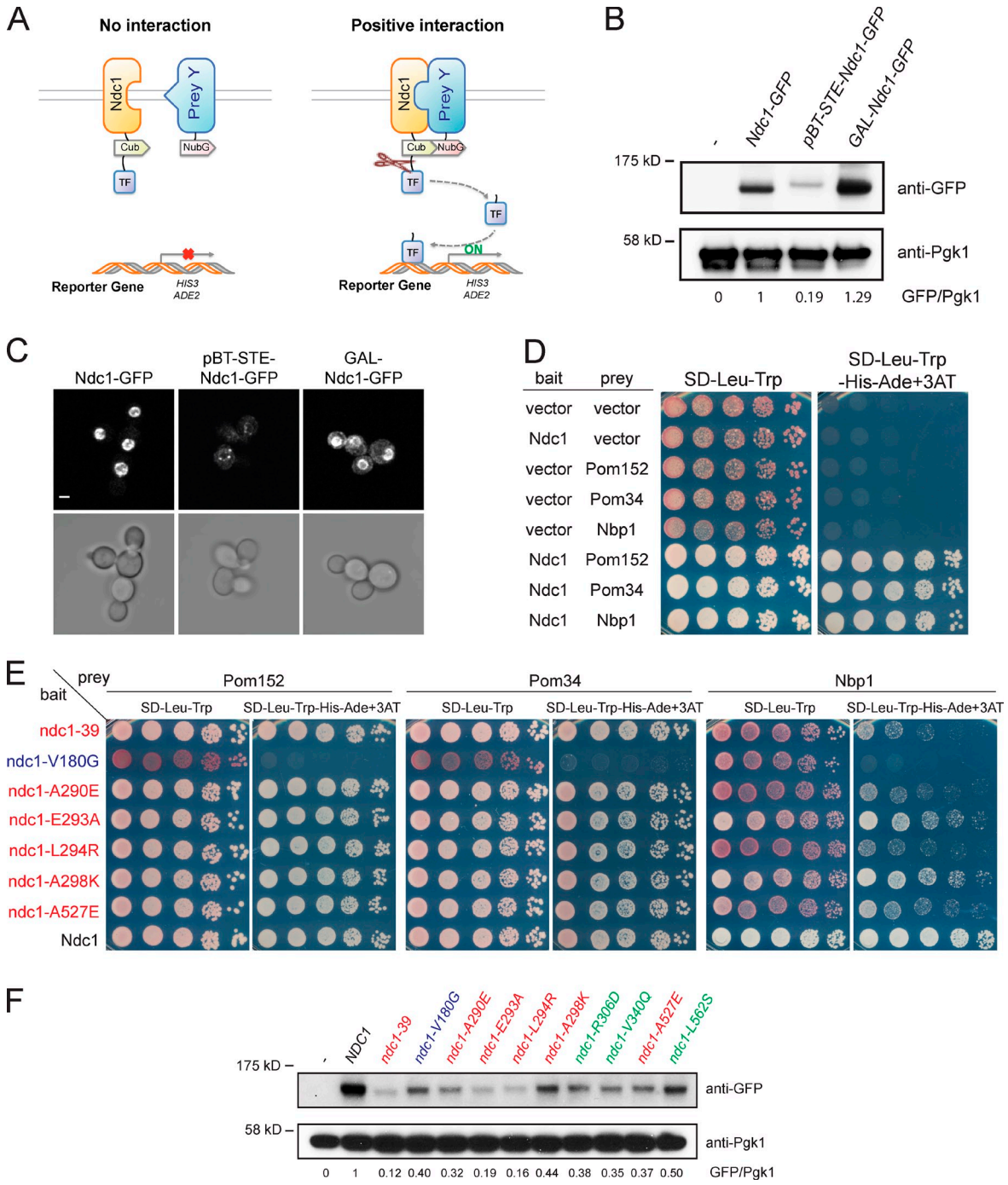


Figure 1. **Identification of new *NDC1* alleles unable to bind to SPB and NPC components.** (A) Schematic of MYTH system used to assay interaction with Ndc1. Prey proteins are fused to the N terminus of ubiquitin (NubG) and expressed along with the bait plasmid containing *NDC1* fused to the C terminus of ubiquitin (Cub) and the LexA-VP16 transcription factor (TF) in yeast cells (SLJ5572) containing the reporter genes *ADE2* and *HIS3*. If Ndc1 is able to interact with the prey, a functional ubiquitin is recognized by ubiquitin proteases that cleave the TF; the soluble TF activates gene expression, which is detected by cell growth on media lacking histidine and adenine. (B and C) Mid-log phase cells producing Ndc1-GFP from the endogenous locus (SLJ6881), the MYTH bait plasmid (SLJ7484), or from the *GAL1* promoter (SLJ7848) were analyzed after a 2-h induction in 2% galactose/2% raffinose-containing media. In B, protein levels in whole-cell lysates were determined by Western blotting with anti-GFP antibodies. Pgk1 served as a loading control and allowed for normalization of the levels of the baits. The strain containing an empty vector (−) was assigned a value of 0 whereas the strain containing Ndc1-GFP expressed from the endogenous locus was given a value of 1. In C, the same strains were imaged to determine to localization of the Ndc1-GFP. Bar, 2 µm. (D and E) Prey plasmids containing the NPC components *POM152* or *POM34* or the SPB component *NBP1* were tested in combination with bait plasmids containing no insert (vector), wild-type *NDC1*, or point mutations in *NDC1* as indicated (see Fig. S1 and Fig. S2 A). *ndc1-39* (T14M, F218V, L288M, E293G, M457T, and F643L) is a ts mutant defective in SPB duplication and NPC assembly (Lau et al., 2004). The presence of both bait and prey plasmids was detected on SD-Leu-Trp media, and activation of the reporters in MYTH was assayed on SD-Leu-Trp-His-Ade plus 3-AT, which reduces background by selecting for robust expression of *HIS3*. 10-fold serial dilutions of cells were spotted onto plates that were incubated for 3 d at 30°C and then placed at 4°C overnight. In E, mutants described in the text and summarized in Table 1 are highlighted. Blue is used for the allele that is unable to bind to Pom34, Pom152, Nbp1, and Mps3; red is used for alleles that are unable to bind Nbp1 and Mps3 but bind to Pom152 and Pom34. (F) Bait proteins were fused to GFP so that their expression and localization could be examined as in B.

Table 1. **Phenotypes of new *NDC1* alleles**

| | Binding by MYTH[a] | | | Growth on 5-FOA[b] | |
|---|---|---|---|---|---|
| **Genotype** | **Pom34** | **Nbp1** | **Mps3** | ***POM152*** | ***pom152Δ*** |
| *NDC1* | ++ | ++ | + | ++ | ++ |
| *ndc1-V180G* | − | − | − | − | − |
| *ndc1-A290E* | ++ | −/+ | − | ts | ts |
| *ndc1-A527E* | ++ | −/+ | − | ++ | ND |
| *ndc1-A298K* | ++ | + | − | − | − |
| *ndc1-L294R* | ++ | −/+ | − | − | − |
| *ndc1-E293A* | ++ | + | − | − | − |
| *ndc1-R306D* | ++ | ++ | − | ++ | ++ |
| *ndc1-V340Q* | ++ | ++ | − | − | − |
| *ndc1-L562S* | ++ | ++ | −/+ | − | ++ |

ND, not determined.
[a]++, indicates robust binding; +, indicates binding; −/+, indicates weak binding; −, indicates no binding.
[b]++, indicates growth at all temperatures; −, indicates no growth at all temperatures; ts, indicates growth at 23°C but not 37°C.



### Mutation of conserved Ndc1 residues

Having established a system to study Ndc1 interactions with both NPC and SPB proteins, we next wanted to determine which regions of Ndc1 were important for its binding to either complex. Because Ndc1 is an integral membrane protein and its insertion, topology, and organization in the membrane are critical to its function, deletion mutants would most likely result in an unfolded protein. Therefore, we created a series of single point mutations in highly conserved residues within non-transmembrane regions of *NDC1* (Fig. S1).

Of the 28 new mutants, we found that only one, ndc1-V180G, was defective in binding to the NPC components Pom152 and Pom34. The ndc1-V180G mutant also fails to bind to the SPB protein Nbp1 (Fig. 1 E, Fig. S2 A; Table 1). Although expression levels of ndc1-V180G are decreased compared with wild-type Ndc1 in the MYTH system (Fig. 1 F; Fig. S2 B), this change is unlikely to explain the mutant's inability to interact with Pom152, Pom34, or Nbp1. ndc1-R287L protein levels are roughly equivalent to ndc1-V180G and binding to all three preys was easily detected (Fig. S2 B). It is probable that ndc1-V180G is nonfunctional due to defects in targeting, post-translational modification, or folding, for example, such that ndc1-V180G is unable or unavailable to associate with preys on the NE. Not surprisingly, the *ndc1-V180G* allele is nonfunctional when it is introduced into yeast (Fig. 2 A; Table 1). Presumably, cells containing *ndc1-V180G* have both NPC and SPB assembly defects similar to the phenotype observed in cells depleted for *NDC1* (Madrid et al., 2006).

### Ndc1 residues important for SPB duplication

Five of our 28 *ndc1* mutants were able to interact with Pom152 and Pom34 as well as wild-type Ndc1 in the MYTH system but showed defects in binding to Nbp1 (Fig. 1 E; Fig. S2 A; Table 1). Importantly, the inability to interact with Nbp1 does not correlate with expression of the allele in the MYTH system (Fig. 1, E and F). This pattern of binding, similar to *ndc1-39*, suggests that these mutants most likely have a defect in SPB duplication. To test this, we integrated these alleles in single copy into a yeast strain containing a deletion of *NDC1* at the genomic locus covered by a wild-type copy of *NDC1* on a *URA3*-based centromeric plasmid. The ability of each allele to serve as the sole copy of *NDC1* was tested by growing cells on 5-fluoroorotic acid (5-FOA), which selects for cells that have lost the p*URA3-NDC1* plasmid (Fig. 2 A; Table 1). Three of these alleles, *ndc1-E293A*, *ndc1-L294R*, and *ndc1-A298K*, are lethal. One allele, *ndc1-A527E*, is viable at all temperatures examined, and the fifth allele, *ndc1-A290E*, exhibits a temperature-sensitive (ts) growth phenotype. Using their expression in the MYTH system as an approximate guide to the expression/stability of these mutants in the cell, the severity of the growth phenotype (viable, ts, lethal) corresponds to abundance of the mutant protein with the exception ndc1-A298K (Fig. 1 F; Fig. S2 B).

Further characterization of *ndc1-A527E* and *ndc1-A290E* revealed several phenotypes consistent with defects in SPB duplication. Although the *ndc1-A527E* mutant does not arrest during the cell cycle, flow cytometric analysis of DNA content showed that the mutant exhibits a partial increase in ploidy at all temperatures, which is common to many SPB duplication mutants (Fig. 2 B). The *ndc1-A290E* mutant is enriched in large-budded cells (71% compared with 38% in wild-type) at the permissive temperature of 23°C and shows a mitotic arrest with monopolar spindles when cells are shifted to the nonpermissive temperature of 37°C for 4 h (Fig. 2, B–G). Indirect immunofluorescence microscopy with anti–α-tubulin (Tub1) and anti–γ-tubulin (Tub4) antibodies to visualize microtubules and SPBs, respectively, showed that ∼90% of large-budded wild-type cells contained a bipolar spindle in which two SPBs were connected by microtubules at both 23 and 37°C. At 23°C, only 59% of large-budded *ndc1-A290E* mutants assembled a bipolar spindle and the remaining 41% contained a monopolar spindle: a single microtubule aster nucleated by one SPB and associated with one mass of DNA. At 37°C, 63% of large-budded *ndc1-A290E* cells have a monopolar spindle (Fig. 2 D; $n = 200$).

Examination of *ndc1-A290E* mutants by serial thin-section electron microscopy (EM) also showed a defect in SPB duplication. A single SPB was found in 29 of 33 (88%) nuclei examined. Of the 29 monopolar spindles, 18 SPBs lacked a recognizable

half-bridge/bridge (Fig. 2 E). In 11 of the 29 monopolar spindles, there is evidence of a cytoplasmic duplication plaque (the precursor to the new SPB) adjacent to the old SPB (Fig. 2 F) or a "dead" pole on an NE extension (Fig. 2 G) in addition to the mother SPB, similar to phenotypes reported for both *ndc1-1* and *ndc1-39* mutants (Winey et al., 1993; Lau et al., 2004). The distribution and morphology of NPCs in *ndc1-A290E* observed by EM and by localization of Nup49-mCherry was indistinguishable from the wild type (Fig. 2, E–H). Based on these data, we conclude that *ndc1-A290E* is defective in SPB duplication.

### The lethality of *ndc1-L562S* is due to a defect in SPB duplication

Mutation of 22 highly conserved residues did not affect Ndc1's interaction with Pom152, Pom34, or Nbp1 based on the MYTH system (Fig. S2 A; Fig. S3 A). We anticipated that all of these alleles would be fully functional because they are able to associate with key Ndc1-binding proteins at both the SPB and NPC. However, two alleles, *ndc1-L562S* and *ndc1-V340Q*, were lethal at all temperatures (Fig. 3 A; Table 1). Further analysis of ndc1-L562S showed that it binds to two additional Ndc1-interacting partners at the NPC, Nup59 and Yop1 (Fig. S3B; Uetz et al., 2000; Casey et al., 2012).

To examine the arrest phenotype of lethal *NDC1* alleles, we created a strain in which a wild-type copy of *NDC1* was fused to GFP and placed under the control of the *GAL1* promoter integrated at the *LEU2* locus. *NDC1* or *ndc1-L562S*, expressed using the *NDC1* promoter, were present at the *NDC1* locus. In galactose-containing media, *NDC1-GFP* is expressed, resulting in growth of both *NDC1* and *ndc1-L562S* strains; in glucose-containing media, expression of *NDC1-GFP* is repressed and *NDC1* strains are viable but *ndc1-L562S* cells are unable to grow, which is consistent with our results using a plasmid shuffle (Fig. 3, A and B). *NDC1-GFP* overproduction results in mislocalization from the NPC and SPB to the ER membrane (Fig. 3 J) and has previously been shown to disrupt SPB duplication (Chial et al., 1999). However, when we examined spindle structure using GFP-Tub1 and Spc42-mCherry, we observed bipolar spindles (Fig. 3, D and E; and unpublished data), which is consistent with the ability of these cells to divide in both liquid culture and on plates (Fig. 3, B and C; Madrid et al., 2006).

At 6, 12, 18, and 24 h after repression of *NDC1-GFP*, the *NDC1* strain continued to divide and bipolar spindles were observed in most large-budded cells (Fig. 3, C–E). In contrast, *ndc1-L562S* cells exhibited an increase in ploidy and eventually arrested in mitosis, as determined by flow cytometric analysis of DNA content, budding index, spindle, and nuclear structure (Fig. 3, C–E). At 12 h, ∼60% of large-budded *ndc1-L562S* cells contained a bipolar mitotic spindle; the remaining 40% of cells contained monopolar spindles (Fig. 3, D and E). By 24 h after repression of *NDC1-GFP*, only 15% of *ndc1-L562S* nuclei contained bipolar spindles. The remaining nuclei primarily contained two SPB foci; however, only one of the SPBs appeared to associate with microtubules (Fig. 3, D and E). To confirm that *ndc1-L562S* had a defect in SPB duplication, serial thin sections of nuclei at the 24-h stage were examined by EM. Consistent with our fluorescence data, most (15 of 19) mitotic nuclei from *NDC1*-containing cells had bipolar spindles (Fig. 3 F). In contrast, only 3 of 30 nuclei from *ndc1-L562S* had evidence of a bipolar spindle (Fig. 3 G); the remaining 27 nuclei contained a single SPB that was often located on a NE invagination (Fig. 3 H). Some were associated with electron-dense particles that may be an SPB precursor such as a satellite or duplication plaque (Fig. 3 I). Examination of NPC structure and distribution using Nup49-mCherry and EM showed that NPCs remain intact throughout the time course (Fig. 3, F–J), suggesting that the defect in SPB duplication occurs before NPC assembly defects. In *ndc1-L562S* mutants, nuclear morphology became irregular in many cells, particularly at later time points. This phenotype is most likely due to enlargement of the vacuole that occurs during the prolonged growth arrest. Therefore, the primary reason for the growth arrest of *ndc1-L562S* is an SPB duplication defect. Because ndc1-L562S is able to interact with Nbp1, these results suggest that Ndc1 has additional binding partners that are important for SPB duplication.

### Ndc1 binds to Mps3

Using the MYTH system, we tested if Ndc1 binds to other SPB components. In addition to interacting with Nbp1, we found that Ndc1 associated with the integral membrane protein Mps3 (Fig. 4, A and B). Ndc1 did not interact with other membrane components of the SPB such as Mps2 or Kar1, nor did it associate with other soluble SPB components such as Bbp1, Cdc31, Sfi1, Cnm67, Spc29, or Spc42 (Jaspersen and Winey, 2004; Winey and Bloom, 2012). Importantly, we found that ndc1-L562S showed only a weak interaction with Mps3 (Fig. 4 C; Table 1), suggesting that a deficiency in Mps3 binding may underlie the SPB duplication defect observed in the *ndc1-L562S* mutant cells. Mutation of other Ndc1 residues, including V340Q and several sites important for Nbp1 binding to Ndc1 such as V180G, A290E, E293A, L294R, and A527E completely abolished binding to Mps3 (Fig. 4 C; Table 1). This finding raises an important question: why do alleles such as *ndc1-A290E*, *ndc1-R306D*, and *ndc1-A527E* that abolish Mps3 binding not phenocopy *ndc1-L562S* and result in lethality? Two notable differences exist between alleles represented by *ndc1-A290E* and the *ndc1-L562S* mutant. The first is binding to Nbp1 in the MYTH system—there is little binding with ndc1-A290E but wild-type levels with ndc1-L562S (Fig. S2 A; Table 1). The second difference is that ndc1-L562S weakly associates with Mps3 in the MYTH system, whereas no interaction was detected with ndc1-A290E (Fig. S2 A). Therefore, we hypothesized that the differences in growth and SPB duplication we observed in *ndc1-A290E* and *ndc1-L562S* were directly attributable to the ability of each allele to associate with Nbp1 or Mps3.

To test this idea, we took advantage of a previously described allele of *NDC1*, *ndc1-39*, which has defects in SPB duplication and NPC assembly due to multiple mutations throughout the protein (Lau et al., 2004). At the semi-permissive temperature of 30°C, ndc1-39 primarily interacts with Nbp1 but not Mps3. However, we can reverse the binding preference by deletion of *POM152* (Fig. 4 D; Table 2). A comparison of the growth of *ndc1-39* and *ndc1-39 pom152Δ* mutants at 30°C showed that

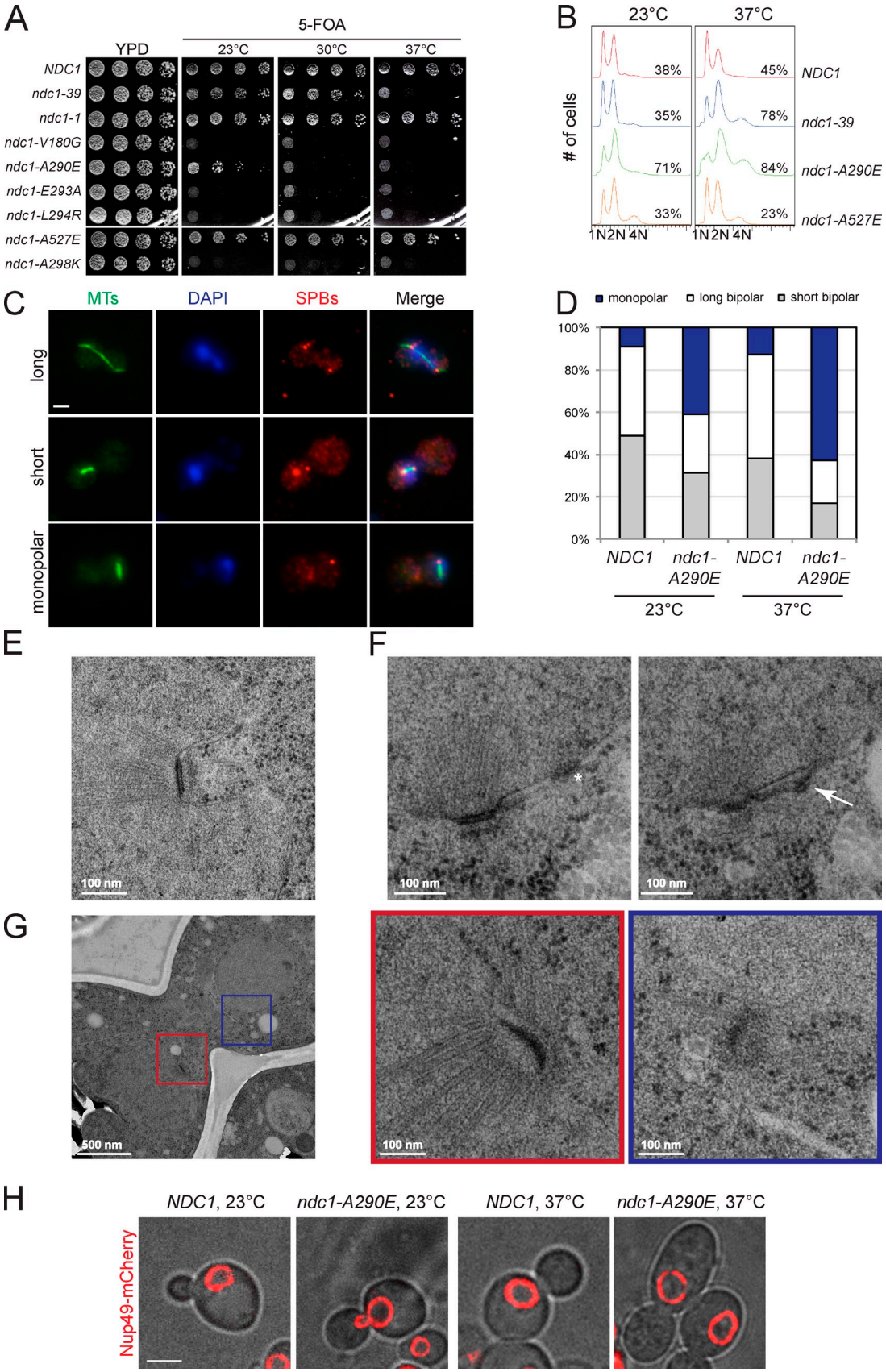


Figure 2. ***ndc1-A290E* is defective in SPB insertion.** (A) The ability of *NDC1* and other alleles of *ndc1* to rescue growth of *ndc1Δ* (SLJ6064) was tested by plating 10-fold serial dilutions of cells onto YPD or 5-FOA, which selects for cells that have lost the p*URA3-NDC1* covering plasmid. Plates were incubated for 2 d at 30 and 37°C and for 3 d at 23°C. (B) Wild-type *NDC1* (SLJ6166), *ndc1-39* (SLJ6167), *ndc1-A290E* (SLJ6170), and *ndc1-A527E* (SLJ6176) were grown in YPD at 23°C or shifted to 37°C for 4 h. DNA content was analyzed by flow cytometry and budding index was determined using

deletion of *POM152* enhances the growth defect of *ndc1-39* at 30°C (Fig. 4 E; Table 2). Based on this finding, together with previously reported SPB defects in *ndc1-39* (Lau et al., 2004), it appears that Nbp1 binding is required for SPB duplication. The idea that Nbp1 is the receptor for Ndc1 at the SPB is consistent with previous reports (Araki et al., 2006). These data also suggest that Mps3–Ndc1 binding is not sufficient for growth and presumably SPB duplication. Moreover, Mps3–Ndc1 binding results in a fitness disadvantage, which is similar to the lethality of *ndc1-L562S*. Alleles that cannot bind to Mps3 do not suffer this growth penalty, although they may still have SPB duplication defects due to an inability to associate with Nbp1.

### Deletion of *POM152* rescues *ndc1-L562S* by increasing its levels at the SPB

If Mps3 does not serve as a SPB receptor for Ndc1, why does a reduction of Mps3 binding to *ndc1-L562S* mutants result in an SPB duplication defect? The localization of Mps3 and Ndc1 not only to the SPB but also to the NE (Chial et al., 1998; Jaspersen et al., 2002) and a series of genetic interactions between SPB and NPC mutants including *MPS3* and *NDC1* (Chial et al., 1998; Jaspersen et al., 2006; Sezen et al., 2009; Witkin et al., 2010; Casey et al., 2012) led us to consider the hypothesis that Mps3 binding to Ndc1 is important for controlling Ndc1 distribution between the SPB and NPCs. We reasoned that if the ndc1-L562S mutant protein is unable to redistribute itself from the NPC to the SPB due to its weak association with Mps3, then the mutant would display profound defects in SPB duplication and ultimately die due to chromosome segregation errors, which we observed (Fig. 3). The model that Mps3 partitions Ndc1 between the NPC and SPB leads to several testable predictions. First, levels of ndc1-L562S at the SPB should be low—presumably below a critical threshold for successful SPB duplication. Second, increasing ndc1-L562S levels at the SPB by overexpression should alleviate the growth defect of *ndc1-L562S* mutants. The temperature sensitivity of *mps3* mutants may also be suppressed by increased expression of *NDC1* but not *ndc1-L562S*. Lastly, if Mps3 is important to partitioning Ndc1 between the NPC and SPB, we would anticipate that binding between Ndc1 or ndc1-L562S and Mps3 would increase in the absence of Pom152, which is one of the primary factors that tethers Ndc1 to the NPC (Onischenko et al., 2009).

To examine the distribution of Ndc1 and ndc1-L562S in cells, *NDC1* and *ndc1-L562S* were fused to GFP in strains containing Spc42-mCherry as well as p*LEU2-NDC1*, which is essential for proliferation of *ndc1-L562S-GFP*–containing cells. Ndc1-GFP and ndc1-L562S-GFP were visualized by fluorescence microscopy and the signal intensity at the SPB was quantitated based on colocalization with Spc42-mCherry. Levels of Ndc1-GFP and ndc1-L562S-GFP on the NE were also quantified, and the abundance of both proteins in lysates was determined by Western blotting. Consistent with previous reports, Ndc1-GFP was observed at the SPB as well as at the NE throughout the cell cycle (Fig. 5 A and Fig. S4) (Chial et al., 1998). As predicted by our genetic data, ndc1-L562S-GFP levels were dramatically reduced at the SPB and NE compared with Ndc1-GFP (Fig. 5, A–C; Fig. S4). This could be caused by decreased expression and/or changes in ndc1-L562S-GFP stability due to its inability to associate with Mps3. It is not known if the NE pool of Ndc1 exchanges with the SPB-associated version throughout the cell cycle.

Two lines of evidence strongly suggest that the SPB duplication defect associated with *ndc1-L562S* is the result of insufficient levels of the mutant protein at the SPB. First, increasing the copy number of *ndc1-L562S* from a single genomic copy to multiple copies using a 2µ plasmid, which is present in ∼5–50 copies per cell, allowed *ndc1-L562S* to serve as the sole copy of *NDC1* at 16, 23, and 30°C (Fig. 5 D). *2µ-ndc1-L562S* only partially restores growth at 37°C, possibly due to folding defects at higher temperatures or due to temperature-dependent changes in the NE that affect SPB duplication. Second, deletion of *POM152* resulted in a small but statistically significant increase in the SPB-associated levels of both Ndc1-GFP and ndc1-L562S-GFP (Fig. 5, A–D). This change in ndc1-L562S levels and distribution in the absence of *POM152* resulted in a complete rescue of the growth and SPB duplication defects observed in *ndc1-L562S* mutants (Fig. 4 E; unpublished data). Interestingly, deletion of other nucleoporins involved in NPC membrane anchoring such as *POM34*, *NUP157*, and *NUP170* did not suppress the growth defect of *ndc1-L562S* (Fig. S3 C). Only *nup42Δ* partially rescued *ndc1-L562S*. This nonessential FG-Nup is a component of the central channel of the NPC, and its removal was previously reported to rescue the growth defect of *mps3-1* (Witkin et al., 2010). It seems likely that suppression by *nup42Δ* occurs through an indirect mechanism, possibly by altering transport of components needed for SPB assembly because Nup42 has no known interaction with any membrane components of the NPC (Aitchison and Rout, 2012). Taken together, these data suggest that a critical threshold of Ndc1 at the SPB is required for SPB duplication. When combined with our observation that the growth defect of *mps3-1* was suppressed by overexpression of *NDC1*, but not *ndc1-L562S* (Fig. 5 E), these

phase-contrast microscopy. The percentage of large-budded cells is indicated ($n$ = 300). (C and D) In addition, spindle morphology was examined using indirect immunofluorescence microscopy using anti–α-tubulin (green), anti–γ-tubulin (red), and DAPI (blue). In C, representative images of large-budded cells with short and long bipolar and monopolar (from SLJ6170) spindles are shown. Bar, 2 µm. In D, the percentage of large-budded cells ($n$ = 200) with bipolar and both types of monopolar spindles is indicated for each strain. (E–G) Serial sections through nuclei of 33 *ndc1-A290E* mutant cells shifted to 37°C for 4 h were examined by EM: 18 nuclei contained a single unduplicated SPB as depicted in E, which in many cases was on an NE invagination as shown, and 11 nuclei contained a monopolar SPB with a nonfunctional second SPB-like structure (F and G). In F, electron dense material (arrow) resembling an SPB duplication plaque or satellite was observed at the end of a bridge. An associated NPC (asterisk) was also detected in the vicinity of the SPB. The abnormally shaped nucleus in G contains an SPB (red) as well as an SPB-like structure (blue) on a NE extension that is associated with cytoplasmic microtubules. Presumably, this is a duplication plaque that has failed to insert into the NE, similar to other "dead" poles previously described. Bar, 100 nm, or indicated. (H) Representative images showing Nup49-mCherry distribution in *NDC1* (SLJ6795) and *ndc1-A290E* (SLJ7486) cells grown at 23°C or shifted to 37°C for 4 h.

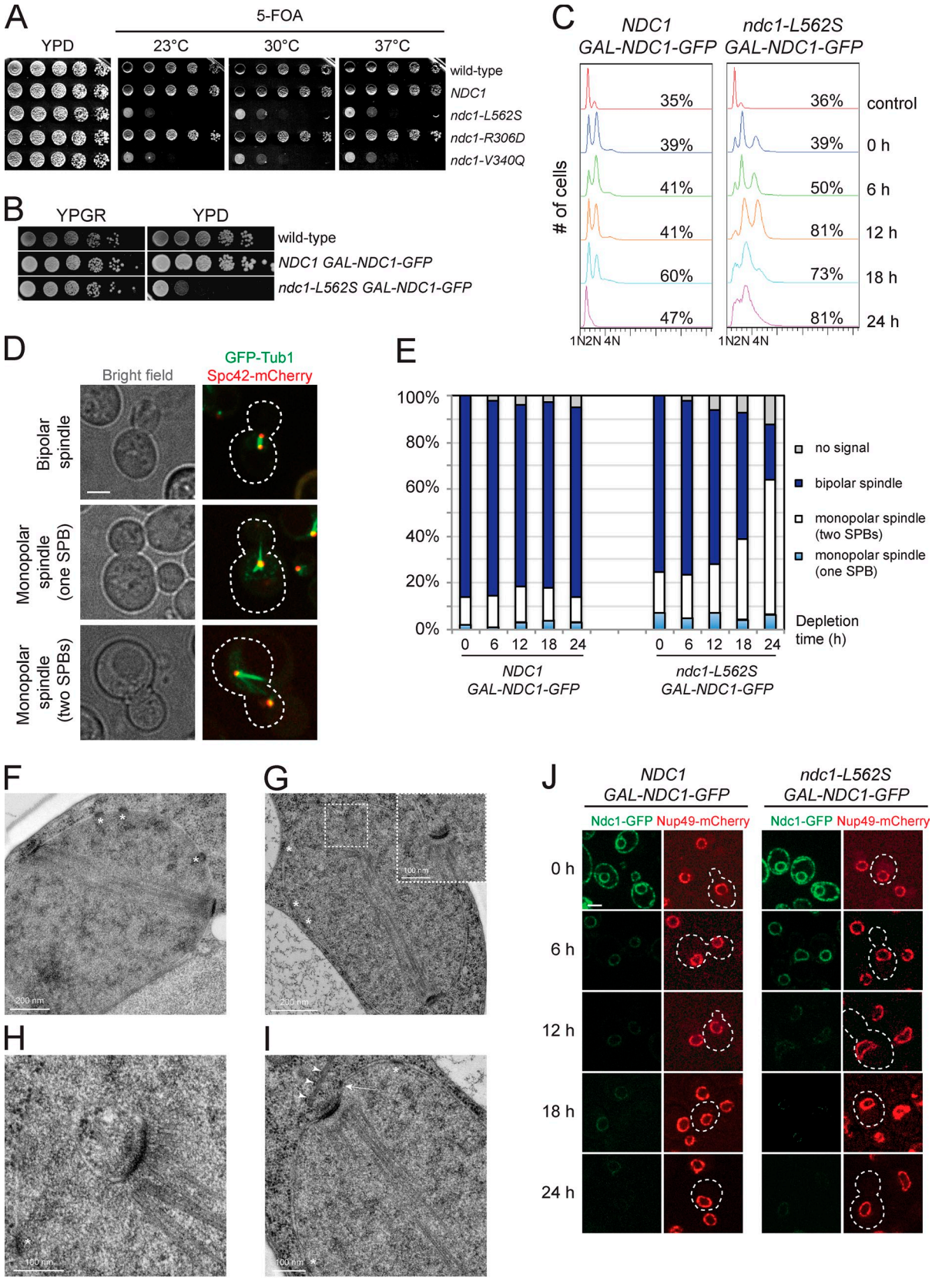


Figure 3. **The *ndc1-L562S* allele is lethal due to a defect in SPB duplication.** (A) Growth of *ndc1Δ* (SLJ6064) cells containing *NDC1* or the indicated alleles was tested by plating 10-fold serial dilutions of cells onto YPD or 5-FOA. Plates were incubated for 2 d at 30 and 37°C and for 3 d at 23°C. (B) Wild-type (SLJ001) cells or cells containing *NDC1* or *ndc1-L562S* as well as *GAL-NDC1-GFP* (SLJ6367 or SLJ6369, respectively) were serially diluted onto YPGR or YPD and grown for 3 d at 30°C. (C–F) These same cells, or isogenic derivatives containing Spc42-mCherry and GFP-Tub1 (SLJ6847 or SLJ6847), were grown in YPGR at 30°C then were transferred into YPD to repress expression of *NDC1-GFP*. (C) Flow cytometric analysis of DNA content

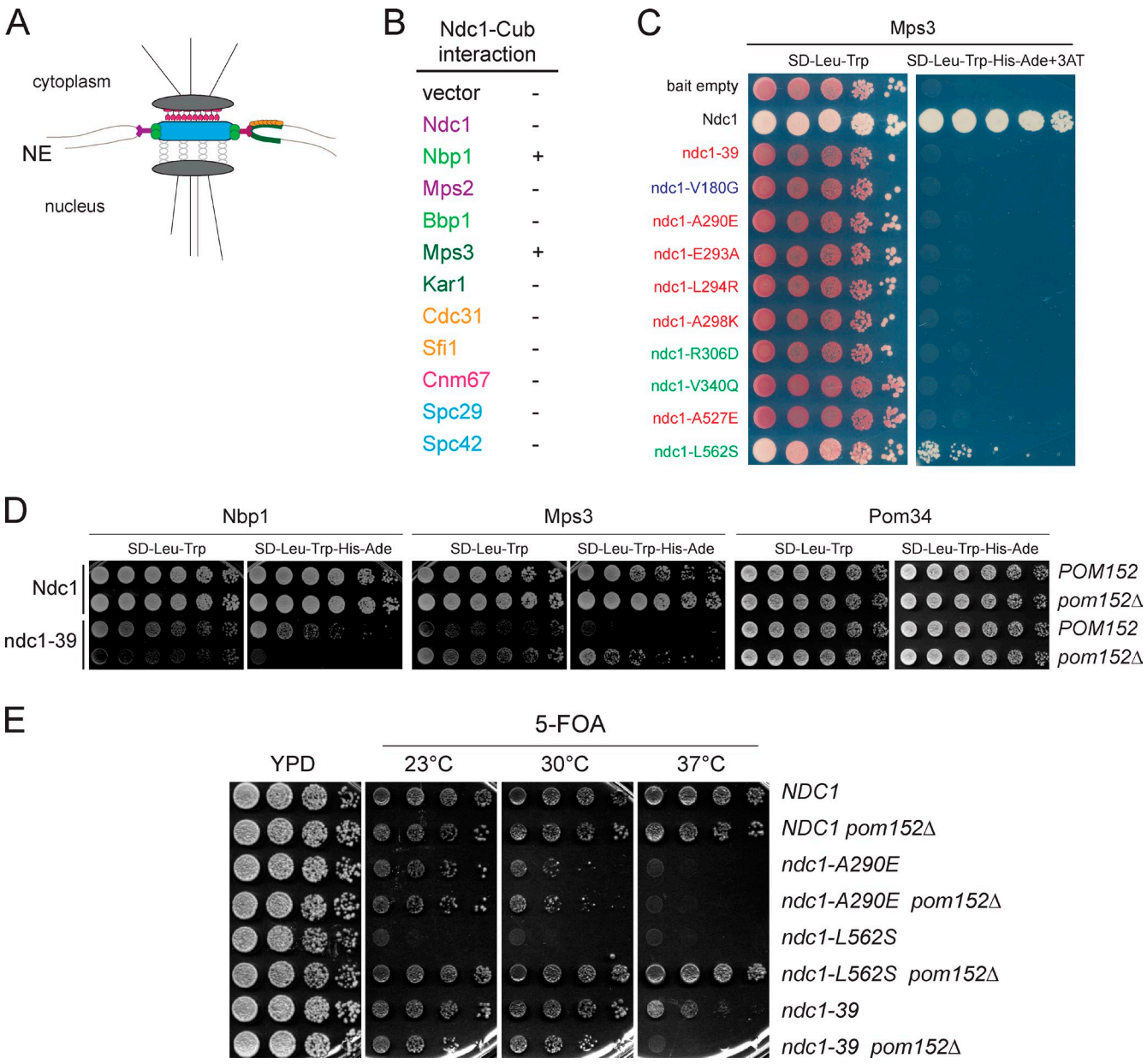


Figure 4. **Mps3 is a novel Ndc1 binding partner.** (A) Schematic of the SPB, showing the soluble central plaque (blue), which is embedded in the NE via Bbp1 and Npb1 (green circles) and their membrane partners Mps2 and Ndc1 (purple), respectively. The half-bridge is composed of the integral membrane proteins Mps3 and Kar1 (green) and the soluble cytoplasmic proteins Cdc31 and Sfi1 (orange). Cnm67 (pink) is a structural component of the SPB that tethers the central plaque to the SPB outer plaque (Jaspersen and Winey, 2004; Winey and Bloom, 2012). (B) Prey plasmids containing the indicated SPB components were tested for their ability to interact with Ndc1 in the MYTH system. "+" indicates an interaction, judged by growth on SD-Leu-Trp-His-Ade; "–" indicates that no interaction was observed. (C) The *MPS3* prey plasmid was tested in combination with bait plasmids containing no insert (vector), wild-type *NDC1*, or point mutations in *NDC1* as indicated using conditions described in Fig. 1. (D) Prey plasmids producing the indicated protein and bait plasmids containing *NDC1* or *ndc1-39* were introduced into wild-type cells used for MYTH (SLJ5572) or a version containing a deletion of *POM152* (SLJ6066). 10-fold serial dilutions of cells were spotted onto SD-Leu-Trp and SD-Leu-Trp-His-Ade and plates were incubated for 2 d at 30°C. (E) Mid-log phase cultures of *ndc1Δ pURA3-NDC1* or *ndc1Δ pom152Δ pURA3-NDC1* cells containing *NDC1* (SLJ6166 or SLJ6178), *ndc1-A290E* (SLJ6170 or SLJ6179), *ndc1-L562S* (SLJ6177 or SLJ6180), or *ndc1-39* (SLJ6167 or SLJ6181) were serially diluted 10-fold and spotted on to YPD or 5-FOA plates that were incubated for 3 d at 23°C or for 2 d at 30 or 37°C.

and budding index were used to assay ploidy and cell cycle arrest at the indicated times. Spindle morphology was examined using GFP-Tub1 (green) and Spc42-mCherry (red). Representative images from large-budded cells are shown in D, and the percentage of cells with bipolar and monopolar spindles was quantitated in E ($n$ = 200). (F–I) Serial sections through nuclei of 19 *NDC1* (SLJ6367) and 30 *ndc1-L562S* (SLJ6369) cells shifted YPD for 24 h were examined by EM: 15/19 and 3/30 nuclei from *NDC1* and *ndc1-L562S* had bipolar spindles as depicted in F and G, respectively. In G, the second SPB found in an adjacent section is shown in the inset. A single SPB was found in 27/30 nuclei from *ndc1-L562S*, often on an NE invagination (H) or associated with material on the NE resembling an intermediate in SPB assembly (I, arrow). Nuclear pore complexes are marked with an asterisk. Bar, indicated. (J) NPC integrity was examined by Nup49-mCherry (red) in SLJ6822 and SLJ6823. Bars, 2 µm.

Table 2. ***POM152* deletion affects growth and binding of *ndc1* mutants**

| | Binding by MYTH[a] | | | Growth on 5-FOA[b] |
|---|---|---|---|---|
| **Genotype** | **Pom34** | **Nbp1** | **Mps3** | |
| *NDC1* | ++ | ++ | + | ++ |
| *pom152Δ* | ++ | ++ | ++ | ++ |
| *ndc1-39* | ++ | −/+ | − | ts |
| *pom152Δ ndc1-39* | ++ | − | + | SS |
| *ndc1-L562S* | ++ | ++ | −/+ | − |
| *pom152Δ ndc1-L562S* | ++ | ++ | ++ | ++ |

SS, synthetic sick.
[a]++, indicates robust binding; +, indicates binding; −/+, indicates weak binding; −, indicates no binding.
[b]++, indicates growth at all temperatures; −, indicates no growth at all temperatures; ts, indicates growth at 23°C but not 37°C.

data strongly support the idea that Mps3 and Ndc1 interact in vivo and this interaction is disrupted in the *ndc1-L562S* mutant.

### Ndc1 binding to Mps3 at the NE is enhanced by deletion of *POM152*

Using the MYTH system, we compared binding of Ndc1 and ndc1-L562S to Pom34, Mps3, and Nbp1 in the presence and absence of *POM152* to better understand how Ndc1 is distributed between NE complexes. Deletion of *POM152* did not affect binding of Pom34 or Nbp1 to either wild-type or the mutant versions of Ndc1 that we tested (Fig. 6 A). Pom152 was also not required for Ndc1 interaction with other proteins such as Yop1 and Nup59. (Fig. S3 B). However, *pom152Δ* significantly enhanced association of ndc1-L562S and Mps3 as well as increased binding of Ndc1 and Mps3 (Fig. 6 A), indicating that Pom152 and Mps3 likely act antagonistically to control the distribution of Ndc1.

This model of Mps3 function in Ndc1 distribution points to the existence of Mps3–Ndc1 complexes on the NE. It also leads to the prediction that the abundance of Mps3–Ndc1 complexes should increase in cells lacking *POM152*. Because of the rapid movement and low concentration of Mps3 at the NE, we were unable to assay binding of Mps3 to Ndc1 at non-SPB sites by fluorescence resonance energy transfer (FRET). Co-immunoprecipitation experiments would also be uninformative because SPB and NE populations cannot be independently analyzed. To demonstrate that Mps3 and Ndc1 form a complex on the NE, we used line-scanning fluorescence cross-correlation spectroscopy (FCCS), which provides spatial and temporal information about intracellular complexes. Unlike FRET, FCCS is not restricted to interactions that are within 10 nm (though it does require co-diffusion), and unlike chemical cross-linking, FCCS can be done in live cells. As depicted in Fig. 6 B, intensity fluctuations of two fluorescently labeled proteins within a focal volume are measured and compared (Schwille et al., 1997; Ruan et al., 2004; Bacia et al., 2006; Ries and Schwille, 2006; Slaughter and Li, 2010). If the labeled proteins are present in a complex, they will synchronously migrate through the focal volume; if the proteins do not associate, their migration will be random. An auto-correlation curve is generated through correlation analysis of the photon counts over time for each individual channel. These data provide information about the number of particles and their rate of diffusion within the focal volume. A cross-correlation curve is also generated by correlation analysis between the two intensity time traces. Information about the protein complex is derived from this analysis—the higher the cross-correlation amplitude relative to the auto-correlation amplitude, the stronger the co-diffusion of the proteins (see Materials and methods).

To determine if Mps3 and Ndc1 form a complex on the NE, cells expressing Ndc1-mTurquoise2 and Mps3-YFP were analyzed. A line profile was selected spanning the NE (Fig. 6 C) and repeated scans of this line on a confocal microscope allowed us to assay the fluctuations of Ndc1-mTurquoise and Mps3-YFP at two NE spots as a function of time. A kymograph of membrane intensity on this line (y axis) versus time (x axis) of a typical FCCS experiment is shown in Fig. 6 D. The two membrane crossing points of our line are seen. Intensity fluctuations are due to diffusion of Ndc1-mTurqouise2 complexes, Mps3-YFP complexes, or complexes containing both proteins along the NE. Auto-correlation curves were generated for both Ndc1-mTurquoise and Mps3-YFP using standard methods. The initial amplitude, G(0), of this correlation curve is inversely proportional to the concentration of protein complexes (Fig. 6 B). The autocorrelation curves decayed on the order of ∼250 ms. This "transit time" represents on average how long it takes the protein to diffuse through the focal volume.

The relative amplitudes of the auto-correlation curves (Fig. 6 E) demonstrates than the concentration of Mps3 particles on the NE is much lower than Ndc1 particles, which is consistent with visual inspection of the cells and simple intensity measurements (Fig. 6 C). The temporal correlation between the channels (cross-correlation) is sensitive to complexes containing both labels; thus, in contrast to auto-correlation, cross-correlation amplitude increases with the number of interacting particles (Bacia et al., 2006; Slaughter et al., 2011). Both wild-type and *pom152Δ* cells have cross-correlation significantly above zero, demonstrating an interaction between mobile Ndc1 and Mps3 complexes at the NE (Fig. 6 E). The non-interacting Mps3-YFP and Ndc1-mTurquoise2 likely represent sites of telomere anchoring and NPC assembly, respectively, where these proteins are not believed to interact (Chial et al., 1998; Bupp et al., 2007; Horigome et al., 2011). These results demonstrate that Mps3 and Ndc1 form a complex on the NE.

To determine if Ndc1 present on the NE is part of the NPC, we analyzed a strain containing Ndc1-mTurquoise2 and

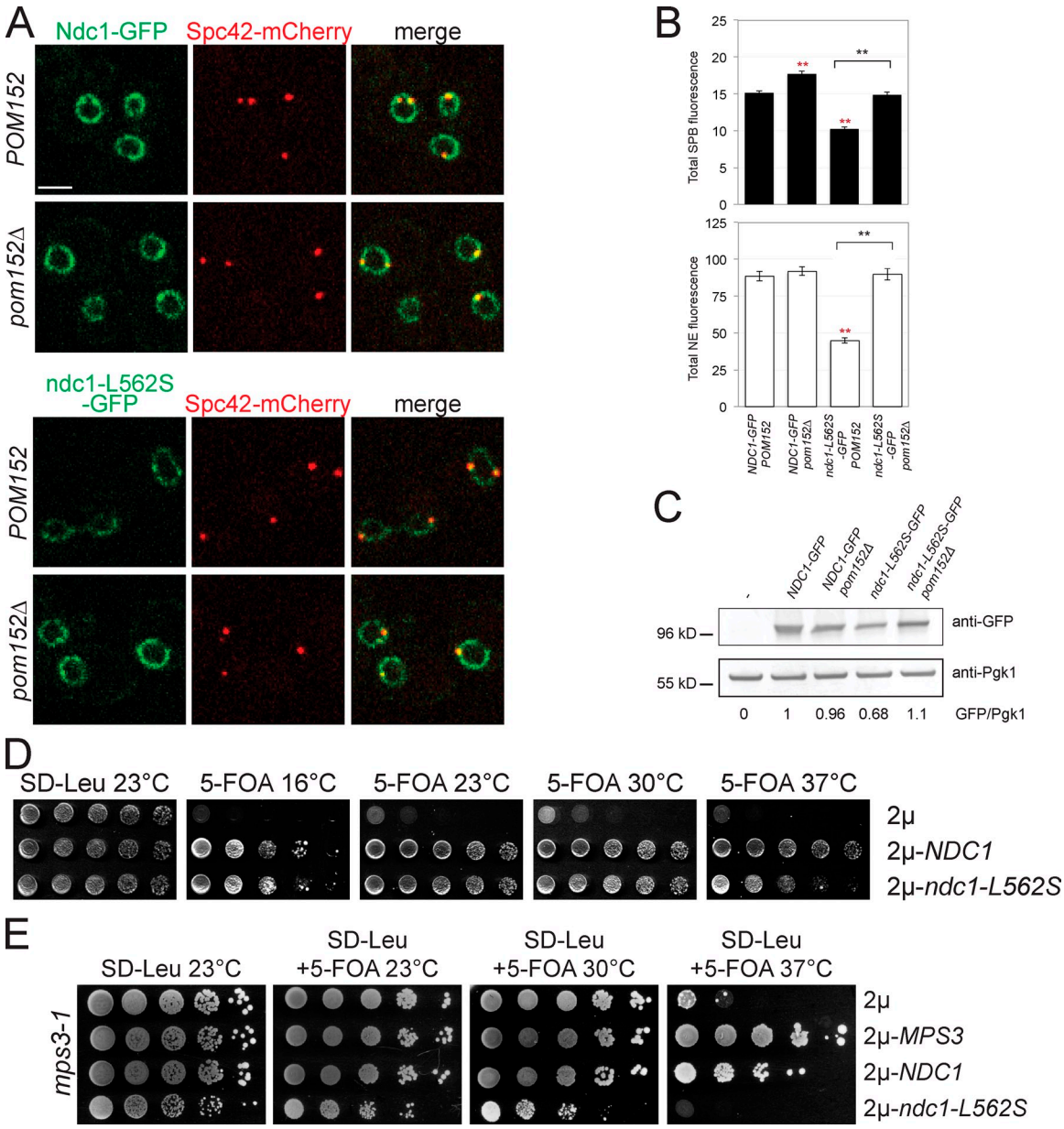


Figure 5. **Increasing levels of *ndc1-L562S* at the SPB rescues the mutant growth defect.** (A–D) Mid-log phase cultures of *ndc1Δ pURA3-NDC1* or *ndc1Δ pom152Δ pURA3-NDC1* cells containing *NDC1-GFP* (SLJ6288 or SLJ6588) or *ndc1-L562S-GFP* (SLJ6638 or SLJ6734) grown in SC-Ura were examined. (A) Representative single plane images showing the localization of Ndc1-GFP or ndc1-L562S-GFP (green), Spc42-mCherry (red), and a merged image. Bar, 2 µm. (B) Levels of Ndc1-GFP or ndc1-L562S-GFP were quantitated as described in Materials and methods, and the average total fluorescence intensity at the SPB and the NE is shown. Error bars depict the SEM. Red and black double asterisks show statistically significant values ($P < 10^{-4}$ using Student's *t* test) compared with wild-type and *ndc1-L562S*, respectively. (C) Extracts were prepared from these cells as well as from control cells lacking a GFP-tagged protein (−). Western blotting using anti-GFP antibodies was used to determine the total levels of Ndc1-GFP or ndc1-L562S-GFP in the cell. Using Pgk1 as a loading control, protein levels were normalized. The control and *NDC1-GFP POM152* cells were assigned values of 0 and 1, respectively. (D) *ndc1-L562S pURA3-NDC1* cells (SLJ6177) transformed with 2µ-*NDC1*, 2µ-*ndc1-L562S*, or an empty plasmid were serially diluted 10-fold and stamped onto SD-Leu or 5-FOA plates that were incubated for 2 d at 30 and 37°C, 3 d at 23°C, and 10 d at 16°C. (E) *mps3-1* (SLJ910) was transformed with the plasmids in D as well as 2µ-*MPS3*, serially diluted 10-fold and stamped onto SD-Leu or SD-Leu plus 5-FOA. Plates were incubated for 2 d at 30 and 37°C and 3 d at 23°C.

Nup49-YFP using the same method. The high degree of cross-correlation observed between these two proteins is consistent with the fact that both are subunits of the NPC (Fig. 6 G; Aitchison and Rout, 2012). Our observation that ∼20% of Ndc1-mTurquoise2 binds to Nup49-YFP compared with the ∼2% observed in a complex with Mps3-YFP illustrates two important points: first, these data confirm the idea that Mps3 is not a subunit of the NPC (Horigome et al., 2011), and second, it shows that Mps3–Ndc1 complexes represent a small pool of both proteins (Fig. 6, F and H). Consistent with our model that the NPC competes with Mps3 for Ndc1 binding, we find that the amount of Ndc1-mTurquoise2–Nup49-YFP complexes decreases (Fig. 6, G and H; $P < 0.0001$), whereas the amount of Ndc1-mTurquoise2–Mps3-YFP increases (Fig. 6 E and F; $P < 0.0001$) in *pom152Δ* mutants.

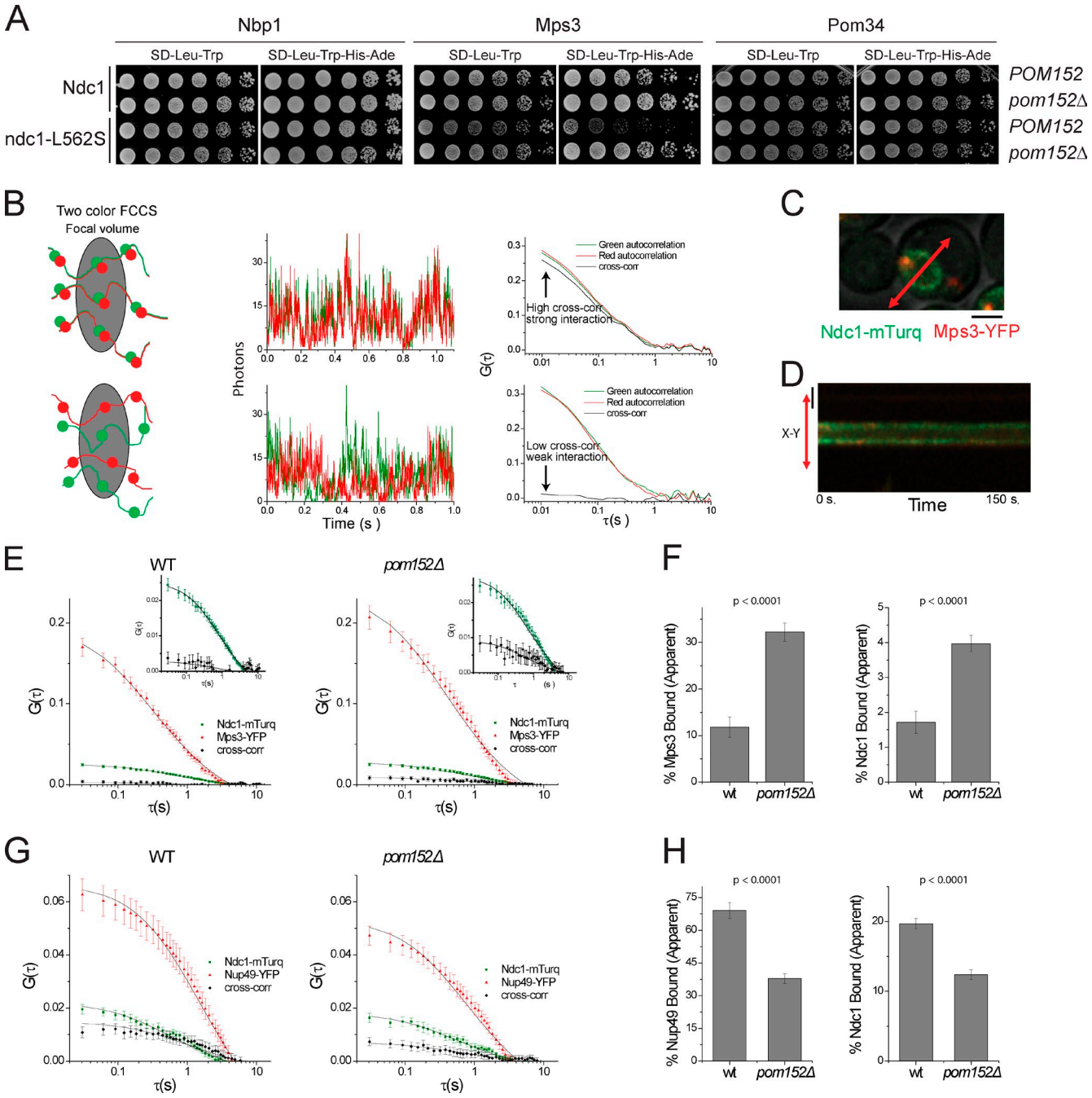


Figure 6. **Mps3 binding to Ndc1 on the NE is antagonized by Pom152.** (A) Prey plasmids producing the indicated protein (Nbp1, Mps3, or Pom34) and bait plasmids containing *NDC1* or *ndc1-L562S* were introduced into wild-type cells used for MYTH (SLJ5572) or a version containing *pom152Δ* (SLJ6066). 10-fold serial dilutions of cells were spotted onto SD-Leu-Trp and SD-Leu-Trp-His-Ade and plates were incubated for 2 d at 30°C. (B) Schematic demonstrating the principle of FCCS. Simulated data and subsequent correlation curves for co-diffusing red and green particles (top) and for randomly diffusing particles (bottom) is shown. The amplitude of the cross-correlation relative to the auto-correlation curves is indicative of the strength of the interaction. (C) A line profile was generated spanning the NE and line-scanning FCCS data were collected in cells containing Ndc1-mTurquoise2 (green) and Mps3-YFP (red). Bar, 2 µm. (D) Each scan along the line can be visualized in a kymograph, which shows at each time point the fluctuations in molecules and complexes as they traverse the NE. Bar, 2 µm. Correlation analysis of intensity fluctuations was performed at the sites where the line-scan crossed the NE. (E) Average auto-correlation and cross-correlation curves and fits are shown for Ndc1-mTurquoise2 and Mps3-YFP in wild-type (SLJ7436) and *pom152Δ* (SLJ7438) cells. Error bars represent the SEM. Inset, magnification of plots to show differences in cross-correlation between strains. (F) The apparent fraction Mps3 and Ndc1 bound is increased in *pom152Δ* cells ($P < 0.0001$). Error bars represent Monte Carlo standard errors. (G and H) FCCS was also analyzed in wild-type (SLJ7835) and *pom152Δ* (SLJ7836) strains containing Ndc1-mTurquoise (green) and Nup49-YFP (red), and analyzed as in E and F. In H, the bound fraction presumably reflects the NPC.

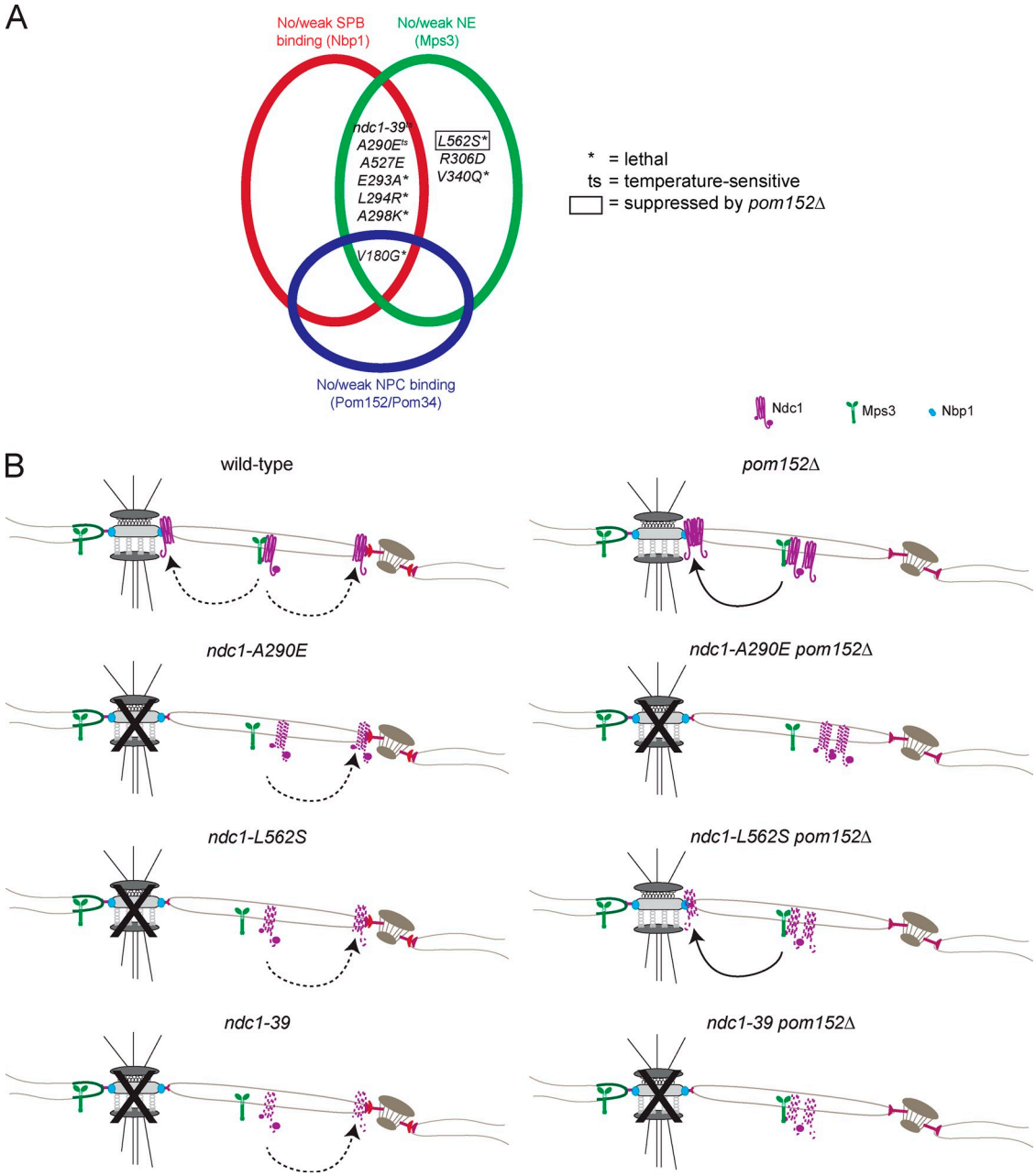


Figure 7. **Model for Ndc1 recruitment to the SPB.** (A) The ability of *ndc1* mutant alleles to bind to Pom34/Pom152, Nbp1, or Mps3 in the MYTH system is contrasted to their growth phenotypes. (B) On the left, in the presence of *POM152*, wild-type Ndc1 associates with Mps3 at NE and is delivered to the SPB so that the new SPB can be inserted in the NE through the Ndc1–Nbp1 interaction. In *ndc1-A290E*, *ndc1-L562S*, and *ndc1-39*, the mutant ndc1 protein cannot bind to Mps3, resulting in an SPB duplication defect. On the right, in cells lacking *POM152*, Ndc1 is released from NPCs, associates with Mps3 at NE, and is delivered to the SPB where it binds to Nbp1. However, an inability of ndc1-A290E to associate with Mps3 results in a failure of the mutant protein to redistribute to the SPB. In contrast, ndc1-L562S released from the NPC can interact with Mps3. Because ndc1-L562S can bind to Nbp1, the growth defect of *ndc1-L562S* is suppressed by *pom152Δ*. In the absence of *POM152*, Mps3 is able to extract ndc1-39 from the NPC more easily, but due to the inability of the mutant protein to associate with Nbp1, cells die due to SPB duplication defects. The mild NPC defect previously reported in *ndc1-39* mutants may be due to sequestration of ndc1-39 in an NE complex with Mps3 that is unavailable for NPC assembly (Lau et al., 2004).

## Discussion

Analysis of conserved residues in the integral membrane protein Ndc1 resulted in the identification of three classes of Ndc1 mutants (Fig. 7 A), including a novel group of mutants represented by *ndc1-L562S* that were lethal despite wild-type interactions with Nbp1, Pom34, and Pom152 in the MYTH system. The lethality of *ndc1-L562S* suggested that Ndc1 bound to at least one additional factor, which we identified as the SUN protein Mps3. Affinity purification of Ndc1 from yeast resulted in copurification of Pom152, Pom34, Nup157, Nup170, and Nup59, as well as Mps3 (Onischenko et al., 2009). This result was attributed to the fact that Mps3 and Ndc1 are both components of the SPB. In this paper, we show that Ndc1 and Mps3 form a complex on the NE. Based on genetic and cytological analysis of wild-type and mutant cells, our data are most consistent

with a model in which Mps3 binding partitions Ndc1 between the SPB and NE (Fig. 7 B).

Examination of multiple *ndc1* alleles allowed us to confirm and extend previous work on the function of Ndc1, Nbp1, and Mps3 during SPB assembly. Cytological, molecular, and genetic characterization of *ndc1-39* and *nbp1-dg* mutants resulted in a model in which Nbp1 serves as a docking protein for Ndc1 at the SPB (Shimizu et al., 2000; Araki et al., 2006; Kupke et al., 2011). An inability to form the Ndc1–Nbp1 connection was observed in mutants such as *ndc1-A290E*. Similar to previously described *ndc1* alleles, this mutant arrests in mitosis at the nonpermissive temperature due to an inability to insert the duplicated SPB into the NE (Winey et al., 1993; Lau et al., 2004). Alleles such as *ndc1-A290E* also fail to associate with Mps3 and are not rescued by *pom152Δ*. The one exception to this rule is *ndc1-39*, which exhibits a synthetic growth defect when combined with *pom152Δ*. The lethality of *ndc1-39 pom152Δ* is most likely not due to an exacerbation of NPC defects as seen in the single mutants but rather is due to sequestration of ndc1-39 in a complex with Mps3 that inhibits ndc1-39 association with Nbp1 (Fig. 7 B).

If Ndc1 binding to Nbp1 is required for SPB duplication, why are mutants such as *ndc1-L562S* lethal? Based on the MYTH system, ndc1-L562S is able to associate with Nbp1 as well as Pom34 and Pom152. We propose that the native ndc1-L562S is kept from interacting with native Nbp1 because it is not efficiently stabilized and distributed between the NPC and SPB due to reduced binding to Mps3. Our data suggest that Mps3 and Pom152 may compete for a shared binding site on Ndc1, which may surround leucine 562. The lethality of *ndc1-L562S* is suppressed by *pom152Δ* because ndc1-L562S binding to Mps3 dramatically increases when *POM152* is eliminated. Association between Mps3 and ndc1-L562S in *pom152Δ* allows for additional mutant protein to be localized to the SPB where it interacts with Nbp1 (Fig. 7 B). Other alleles such as *ndc1-V340Q* and *ndc1-A290E* are not suppressed by *pom152Δ* because Mps3 binding is abolished in those mutants—although mutant ndc1 protein may be released from the NPC, it cannot be distributed to the SPB because of an inability to associate with Mps3.

Ndc1 localizes to the membrane region of both the SPB and NPC, and several genetic interactions have been reported between alleles of *ndc1* and deletion mutants in components of the NPC (Chial et al., 1998; Lau et al., 2004). Thus, Ndc1 is thought to facilitate insertion of SPBs and NPCs into the NE. Consistent with this notion, depletion of Ndc1 results in an ∼40–60% reduction in NPC localization of Nup59, Nup60, and Nup159, as well as reduced levels of nuclear import after 24 h (Madrid et al., 2006). However, these cells arrest with monopolar spindles similar to our *ndc1-L562S* mutants in which *NDC1-GFP* was repressed. It is possible that the NPC defects are a secondary consequence due to titration of the residual Ndc1 away from the NPC to the SPB, raising the question as to whether Ndc1 is required for NPC assembly in budding yeast or if it is partially redundant with Pom152, Pom34, and Pom33, as appears to be the case in the filamentous fungus *Aspergillus nidulans* (Osmani et al., 2006; Liu et al., 2009). Despite considerable mutagenesis of *NDC1*, we were unable to isolate *NDC1* alleles that are specifically defective in NPC assembly, function, or binding. Instead, we only isolated one allele, *ndc1-V180G*, which was unable to bind to Pom152 and Pom34. Located between the fourth and fifth transmembrane domain, this region may define a binding surface for nucleoporins and SPB components because it is near S119N, the residue mutated in *ndc1-1* (Winey et al., 1993). However, it is also possible that mutants in this region may simply affect protein folding or stability, and therefore alter levels of Ndc1.

We showed that Mps3 and Ndc1 interact at unique sites on the NE that are not part of the SPB or NPC. Although only a small fraction of Mps3 and Ndc1 may form these sites, they are important for SPB duplication, perhaps as reservoirs of Ndc1. Binding between Ndc1 and SUN proteins may define an evolutionarily conserved mechanism to regulate the ability of MTOCs to associate with the NE and for the associated MTOC to move within the context of the NE and trigger NE remodeling events such as NE breakdown. Although we cannot rule out the idea that Mps3 and Ndc1 associate at the SPB, our observations indicate that Nbp1, and not Mps3, is the primary receptor for Ndc1 at the SPB. Also consistent with the idea that Mps3–Ndc1 association may not occur at the SPB is immuno-EM localization of Mps3-GFP and Ndc1-GFP to non-identical locations within the SPB (Chial et al., 1998; Jaspersen et al., 2002). Our data illustrate the exquisite sensitivity of yeast to Ndc1 levels. A 40% reduction of ndc1-L562S-GFP at the SPB was associated with lethality due to a defect in SPB insertion into the NE. Increasing the Ndc1 levels by controlling its distribution within the NE or by overexpression of the mutant gene rescues the growth defect of *ndc1* mutants (Chial et al., 1998, 1999). In a similar manner, it is likely that regulation of Ndc1 distribution by SUN proteins at the NE plays a key role in the maintenance of genomic stability in all eukaryotes due to the fact that Ndc1 may dictate sites of NPC assembly and NE anchoring of MTOCs.

## Materials and methods

### Yeast strains and plasmids

All strains are derivatives of W303 (*ade2-1 trp1-1 leu2-3,112 ura3-1 his3-11,15 can1-100 RAD5+*) and are listed in Table S1. Standard techniques were used for DNA and yeast manipulations, including C-terminal tagging of *NDC1* and alleles with GFP. Likewise, fusion of *SPC42* or *NUP49* to mCherry, *MPS3* to YFP, and deletion of genes with *KANMX*, *NATMX*, or *HYGMX* was also done by PCR-based methods (Longtine et al., 1998; Sheff and Thorn, 2004). A yeast codon–optimized version of mTurquoise2, a CFP mimic (Goedhart et al., 2012), was constructed in the *URA3MX* tagging cassette described by Sheff and Thorn (2004), and was used to C-terminally tag *NDC1*. Site-directed mutagenesis was performed by using the QuikChange mutagenesis kit (Agilent Technologies) based on pSJ1287 (pBT3-*STE-NDC1*), pSJ1289 (pRS304-*KANMX-NDC1*), or pSJ1386 (pRS425-*NDC1*; Chial et al., 1999; Lau et al., 2004). Sequencing was performed to confirm correct base pair substitutions or deletions were made.

Bait and prey constructions were generated by amplifying SfiI–SfiI fragments and directionally inserted into the SfiI site of pSJ1283 (pBT3-*STE*) or pSJ1275 (pPR3N). To construct pSJ1386 (pRS425-*NDC1*), the *NDC1* open-reading frame was subcloned into the XmaI and XhoI sites of pRS425 (Sikorski and Hieter, 1989). To induce expression of *NDC1*, we first generated the plasmid pSJ1384 (pRS306-*GAL1-NDC1-GFP*) by inserting the open reading frame of *NDC1* into pSJ114 (pRS306-*GAL1-GFP*; Gardner et al., 2011) at XhoI and HindIII sites. Then the whole *GAL1-NDC1-GFP* cassette was amplified with 5′-GATCGCGGCCGCGGTACCTTATATT-GAATTTTCAAAAAT-3′ and 5′-GATCGAGCTCGAGCTCTTATTTG-TATAGTTCATCCAT-3′ and cloned into pRS305 at NotI and SacI sites to

generate pSJ1380 (pRS305-*GAL1-NDC1-GFP*). Plasmids were digested with EcoNI, BstEII, ApaI, StuI, or PmlI to target integration to *KANMX*, *LEU2*, *URA3*, *ADE2*, or *TRP1*, respectively. Correct integration was confirmed by PCR.

For dilution assays, 5 $OD_{600}$ of cells were spotted in10-fold serial dilutions onto agar plates. YPD has 2% glucose and YPGR has 2% galactose and 2% raffinose as the carbon source. To test for rescue of *ndc1-L562S* (SLJ6177), cells were transformed with 2µ-*LEU2*–based plasmids and transformants were cultured and spotted onto SD-Leu and 5-FOA plates and incubated at 16, 23, 30, and 37°C.

**Membrane yeast two-hybrid system**

Bait plasmids are *LEU2*-marked centromeric plasmids, and prey plasmids are *TRP1*-marked 2µ plasmids. Plasmids were co-transformed into SLJ5572 (NMY51; Dualsystems Biotech) or SLJ6066, then were randomly selected from SD-Leu-Trp plates, cultured, and spotted onto SD-Leu-Trp and SD-Leu-Trp-His-Ade plates and grown for 3–4 d at 30°C. In many cases 10 mM 3-aminotriazole (3-AT) was added to the SD-Leu-Trp-His-Ade plates to prevent leaky expression of *HIS3*, which occurs in this system (Stagljar and Fields, 2002; Thaminy et al., 2003; Snider et al., 2010).

**Cytological techniques**

To analyze the phenotype of *ndc1-L562S*, SLJ6369, and SLJ6367, single colonies were picked from 5-FOA plates containing galactose and raffinose and inoculated into YEP + 2% galactose at 23°C. After overnight growth to mid-log phase, cells were washed with YPD, then inoculated into YPD at 0.1 $OD_{600}$ at 23°C. At 0, 6,12,18, and 24 h after transfer into YPD, the cells were harvested and analyzed by flow cytometry, indirect immunofluorescence microcopy, and/or by live-cell imaging. Cells were considered to be large budded if the bud size was >30% the size of the mother cell.

DNA content was analyzed by flow cytometry in sonicated cells that had been fixed with 70% ethanol for 1 h at room temperature, treated with RNase (Roche) and proteinase K (Roche) for 2 h to overnight at 37°C, and stained with propidium iodide (Sigma-Aldrich) in the dark at 4°C overnight. Samples were analyzed on a MACSQuant FACS Analyzer (Miltenyi Biotec) and data were displayed using FlowJo software (Tree Star).

Spindle integrity was assayed by indirect immunofluorescence microscopy as described previously (Jaspersen et al., 2002). In brief, cells were fixed for 45 min in 4% paraformaldehyde and the SPB and microtubules were stained with 1:500 dilutions of anti-Tub4 and YOL1/34 (Abcam) antibodies, respectively. DNA was visualized by staining with 1 mg/ml DAPI for 5 min immediately before mounting with Citifluor (Ted Pella). Images were captured on an AxioImager (Carl Zeiss) using a 100× αPlan-Fluar objective (NA 1.45; Carl Zeiss) with a digital camera (Orca-ER; Hamamatsu Photonics) and processed using AxioVision 4.6.3 software (Carl Zeiss).

Live-cell imaging was performed on a spinning disk confocal microscope (UltraVIEW; PerkinElmer) equipped with an EM-CCD camera (model C9100-13; Hamamatsu Photonics) optimized for speed, sensitivity, and resolution. The microscope base was an Axio Observer (Carl Zeiss) equipped with an αPlan Apochromat 100×, 1.46 NA oil immersion objective and a multiband dichroic reflecting 488- and 561-nm laser lines. GFP images were acquired with 488 nm excitation and 500–550 nm emission. mCherry images were acquired with 561 nm excitation and 580–650 nm emission. Data were acquired using Volocity software (PerkinElmer) with a z spacing of 0.4 µm. Exposure time, laser power, and camera gain were maintained at a constant level chosen to provide high signal-to-noise but avoid signal saturation for all samples. Images were processed using ImageJ (National Institutes of Health, Bethesda, MD). A representative z slice image is shown.

**Quantitation of Ndc1 distribution**

Quantitation of Ndc1-GFP levels at the NE and SPB was performed with custom plugins (freely available at http://research.stowers.org/imagejplugins) written for ImageJ. Before processing, the average of a manually selected region corresponding to the background was selected from all images. For the identification of SPBs, Spc42-mCherry images were first processed with a maximum projection and 2D smoothing with a 9 × 9-pixel boxcar filter. Background subtraction was then accomplished by subtracting a Gaussian blurred ($\sigma$ = 6 pixels) version of the image from itself. Next, a Sobel edge detection filter was applied and the image was thresholded at 15 times the average intensity. Finally, the thresholded foci were dilated and objects within 30 pixels of the image edge were eliminated. SPB positions in two dimensions were calculated using the centroids of contiguous objects. Manual inspection was performed to eliminate objects not corresponding to valid SPBs. Nuclear masks were created from the Ndc1-GFP signal. First, a sum projection was performed, then the bright 9 × 9-pixel regions corresponding to SPBs were replaced by the average of their surrounding region. The image was then blurred with a Gaussian filter ($\sigma$ = 3 pixels), and nuclei were thresholded locally for 40 × 40-pixel regions surrounding each SPB centroid using a threshold of 0.75 times the intensity surrounding the SPB region. Finally, the SPB intensity was calculated as the sum of the sum projected image in the 5 × 5-pixel region surrounding the SPB centroid and the total NE intensity was calculated as the sum of the same projection over the nuclear mask. It is important to note that our SPB intensity represents a slight overestimate given that nuclear envelope signal is present above and below the SPB. Nevertheless, we reasoned that the SPB represented the vast majority of the signal in this region and that such an approximation would not dramatically alter our results.

**Line-scanning FCCS**

Cells for FCCS were grown to mid-log phase and immobilized between a slide and a coverslip before imaging with a 40×, 1.2 NA Plan Apochromat objective on an imaging device (ConfoCor 3; Carl Zeiss) using the Avalanche photodiode (APD) imaging module. The following parameters were used: mTurquoise2 was excited at 458 nm and emission was collected through a BP 470–495 filter, and YFP was excited at 514 nm and emission collected through a BP 530–575 nm filter. Control experiments demonstrated no back-bleedthrough of YFP into the BP 470–495-nm filter, and no excitation of mTurqouise2 with 514-nm laser light (Goedhart et al. 2012). Thus, with data acquisition in multi-track mode, the system was free of spectral cross talk. Lines through the nucleus were selected to cross a central focal plane perpendicular to the nuclear periphery and away from the SPB (see Fig. 6 C). Line-scan data where the bright SPB traversed the focal volume were easily distinguished and were eliminated from analysis. Line-scanning time series were collected with a line size of 512 pixels and an effective line time for both channels of 15.3 ms. The pixel size was 22 nm, resulting in a total line size of 11.3 µm. The pixel dwell time was 6.4 µs.

Line-scanning kymographs were analyzed using custom software in ImageJ (available at http://research.stowers.org/imagejplugins). Line-scanning cross-correlation analysis was performed following previously published methods (Ries and Schwille, 2006; Ries et al., 2009; Slaughter et al., 2011). In brief, kymographs were binned by 4 pixels in space and 2 lines in time. As nuclei tended to drift slowly in time, profiles tracking the maximum of the NE over time were selected manually from a second kymograph and binned further by 20 lines (see Fig. 6 D). Temporal intensity profiles were then generated for each channel from these tracks, summing over 4 spatial pixels at each time point. In this way, the final profiles have a temporal resolution of 30.6 ms and each time point is the sum of 32 original pixels for a total pixel dwell time of 0.2 ms. Intensity profiles were detrended to correct for bleaching by splitting the dataset into two parts and subtracting a linear fit from each part. The average intensity of the trajectory was then added back to retain the appropriate statistics. Average auto- and cross-correlation curves were generated and fit to a single component diffusion model where diffusion occurs along the axial direction of the focal volume (Ries et al., 2009). Approximately 40 curves were averaged for the *pom152Δ* strain. Noise in the cross-correlation data makes it difficult to accurately fit diffusion time. In addition, the amplitude of the cross correlation is only weakly dependent on the choice of diffusion time. Given that we expect the co-diffusing species to have similar mobility to the independently diffusing species, we fixed the cross-correlation diffusion time to the average of the Mps3-YFP/Nup49-YFP and Ndc1-mTurquoise2 diffusion times. The cross-correlation is reported as the ratio of the cross-correlation amplitude to the Ndc1-mTurquoise2 auto-correlation amplitude. This ratio is proportional to the fraction of Mps3-YFP/Nup49-YFP bound to Ndc1-mTurquoise2 (Bacia et al., 2006; Slaughter et al., 2011).

Errors for auto- and cross-correlation amplitudes were generated by Monte Carlo analysis (Bevington and Robinson, 2003; Das et al., 2012). In brief, 1,000 curves were simulated with Gaussian noise having the same standard deviation as the residuals for each dataset. Each of these curves was fit and the standard deviations of the simulated fit parameters were used as standard errors of each fit parameter. P-values were then calculated according to the normal distribution. Displayed error bars for each point were standard errors in the mean of each averaged correlation point.

**Transmission electron microscopy**

*ndc1-A290E* cells were grown overnight at 23°C and then shifted into a pre-warmed 37°C water bath for 4 h. Cells were quickly harvested and frozen on a high-pressure freezer (EM-Pact; Leica) at ∼2050 bar, transferred

under liquid nitrogen into 2% osmium tetroxide/0.1% uranyl acetate/acetone, and transferred to an automatic freeze substitution (AFS) chamber (Leica). The freeze substitution protocol was as follows: −90° for 16 h, raised 4°/h for 7 h; −60° for 19 h, raised 4°/h for 10 h; and −20° for 20 h. Samples were then removed from the AFS, placed in the refrigerator for 4 h, and then allowed to incubate at room temperature for 1 h. Samples went through three changes of acetone over 1 h and were removed from the planchettes. They were embedded in acetone/Epon mixtures to final 100% Epon over several days in a stepwise procedure as described previously (McDonald, 1999). 60-µm serial thin sections were cut on an ultramicrotome (model UC6; Leica), stained with uranyl acetate and Sato's lead, and imaged on a transmission electron microscope (Tecnai Spirit; FEI).

### Western blotting

Lysates from *NDC1-GFP* or *ndc1-L562S-GFP* cells were prepared from mid-log phase cultures. Pelleted cells were washed in PBS and frozen in liquid nitrogen. Thawed pellets were resuspended in 1 ml lysis buffer (50 mM Tris, pH 7.5, 150 mM NaCl, 0.1%NP-40, 1 mM DTT, 10% glycerol, and 1 mg/ml each pepstatin A, aprotinin, and leupeptin), and ∼100 µl of glass beads were added before bead beating for 1 min × 5 with 2 min on ice between beatings. Samples were spun at 5,000 rpm for 2 min and the supernatant was transferred to a new tube. Protein concentration was determined using a spectrophotometer (NanoDrop; Thermo Fisher Scientific), and equivalent amounts of lysate were analyzed by SDS-PAGE followed by Western blotting. Whole-cell extracts were prepared by bead beating into SDS sample buffer to determine expression levels of baits. The following primary antibody dilutions were used: 1:1,000 anti-GFP (Roche); 1:1,000 anti-Pgk1 (Invitrogen); and 1:1,000 anti-LexA (EMD Millipore). Alkaline phosphatase–conjugated secondary antibodies were used at 1:10,000 (Promega) and horseradish peroxidase–conjugated secondaries were used at 1:1,000 (Cell Signaling Technology).

### Online supplemental material

Fig. S1 shows alignment of *NDC1*. Fig. S2 shows MYTH analysis of *ndc1* alleles. Fig. S3 shows the relationship between *ndc1* mutants and other nucleoporins. Fig. S4 shows levels of *ndc1-L562S* at the SPB and NE during the cell cycle. Table S1 lists yeast strains. Online supplemental material is available at http://www.jcb.org/cgi/content/full/jcb.201307043/DC1.

We are grateful to M. Winey and K. Weis for Ndc1 strains and plasmids. We thank B. Miller, K. Weaver, M. Kirkman, and C. Cahoon for help with construction of mutants and strains; and M. McClain for assistance with EM. We thank M. Winey, S. Hawley, C. Cahoon, and members of the Jaspersen laboratory for comments on the manuscript.

S.L. Jaspersen is supported by the Stowers Institute for Medical Research and the American Cancer Society (RSG-11-030-01-CSM).

The authors declare no competing financial interests.

Submitted: 8 July 2013
Accepted: 6 January 2014

## References

Aitchison, J.D., and M.P. Rout. 2012. The yeast nuclear pore complex and transport through it. *Genetics*. 190:855–883. http://dx.doi.org/10.1534/genetics.111.127803

Alber, F., S. Dokudovskaya, L.M. Veenhoff, W. Zhang, J. Kipper, D. Devos, A. Suprapto, O. Karni-Schmidt, R. Williams, B.T. Chait, et al. 2007. Determining the architectures of macromolecular assemblies. *Nature*. 450:683–694. http://dx.doi.org/10.1038/nature06404

Araki, Y., C.K. Lau, H. Maekawa, S.L. Jaspersen, T.H. Giddings Jr., E. Schiebel, and M. Winey. 2006. The *Saccharomyces cerevisiae* spindle pole body (SPB) component Nbp1p is required for SPB membrane insertion and interacts with the integral membrane proteins Ndc1p and Mps2p. *Mol. Biol. Cell*. 17:1959–1970. http://dx.doi.org/10.1091/mbc.E05-07-0668

Bacia, K., S.A. Kim, and P. Schwille. 2006. Fluorescence cross-correlation spectroscopy in living cells. *Nat. Methods*. 3:83–89. http://dx.doi.org/10.1038/nmeth822

Baker, J., W.E. Theurkauf, and G. Schubiger. 1993. Dynamic changes in microtubule configuration correlate with nuclear migration in the preblastoderm *Drosophila* embryo. *J. Cell Biol.* 122:113–121. http://dx.doi.org/10.1083/jcb.122.1.113

Bevington, P., and D.K. Robinson. 2003. Testing the fit. *In* Data Reduction and Error Analysis for the Physical Sciences. McGraw-Hill, NY. 194–217.

Bigay, J., J.F. Casella, G. Drin, B. Mesmin, and B. Antonny. 2005. ArfGAP1 responds to membrane curvature through the folding of a lipid packing sensor motif. *EMBO J.* 24:2244–2253. http://dx.doi.org/10.1038/sj.emboj.7600714

Bupp, J.M., A.E. Martin, E.S. Stensrud, and S.L. Jaspersen. 2007. Telomere anchoring at the nuclear periphery requires the budding yeast Sad1-UNC-84 domain protein Mps3. *J. Cell Biol.* 179:845–854. http://dx.doi.org/10.1083/jcb.200706040

Byers, B., and L. Goetsch. 1974. Duplication of spindle plaques and integration of the yeast cell cycle. *Cold Spring Harb. Symp. Quant. Biol.* 38:123–131. http://dx.doi.org/10.1101/SQB.1974.038.01.016

Byers, B., and L. Goetsch. 1975. Behavior of spindles and spindle plaques in the cell cycle and conjugation of *Saccharomyces cerevisiae*. *J. Bacteriol.* 124:511–523.

Casey, A.K., T.R. Dawson, J. Chen, J.M. Friederichs, S.L. Jaspersen, and S.R. Wente. 2012. Integrity and function of the *Saccharomyces cerevisiae* spindle pole body depends on connections between the membrane proteins Ndc1, Rtn1, and Yop1. *Genetics*. 192:441–455. http://dx.doi.org/10.1534/genetics.112.141465

Chial, H.J., M.P. Rout, T.H. Giddings, and M. Winey. 1998. *Saccharomyces cerevisiae* Ndc1p is a shared component of nuclear pore complexes and spindle pole bodies. *J. Cell Biol.* 143:1789–1800. http://dx.doi.org/10.1083/jcb.143.7.1789

Chial, H.J., T.H. Giddings Jr., E.A. Siewert, M.A. Hoyt, and M. Winey. 1999. Altered dosage of the *Saccharomyces cerevisiae* spindle pole body duplication gene, *NDC1*, leads to aneuploidy and polyploidy. *Proc. Natl. Acad. Sci. USA*. 96:10200–10205. http://dx.doi.org/10.1073/pnas.96.18.10200

Das, A., B.D. Slaughter, J.R. Unruh, W.D. Bradford, R. Alexander, B. Rubinstein, and R. Li. 2012. Flippase-mediated phospholipid asymmetry promotes fast Cdc42 recycling in dynamic maintenance of cell polarity. *Nat. Cell Biol.* 14:304–310. http://dx.doi.org/10.1038/ncb2444

Dawson, T.R., M.D. Lazarus, M.W. Hetzer, and S.R. Wente. 2009. ER membrane-bending proteins are necessary for de novo nuclear pore formation. *J. Cell Biol.* 184:659–675. http://dx.doi.org/10.1083/jcb.200806174

Ding, R., R.R. West, D.M. Morphew, B.R. Oakley, and J.R. McIntosh. 1997. The spindle pole body of *Schizosaccharomyces pombe* enters and leaves the nuclear envelope as the cell cycle proceeds. *Mol. Biol. Cell*. 8:1461–1479. http://dx.doi.org/10.1091/mbc.8.8.1461

Gardner, J.M., C.J. Smoyer, E.S. Stensrud, R. Alexander, M. Gogol, W. Wiegraebe, and S.L. Jaspersen. 2011. Targeting of the SUN protein Mps3 to the inner nuclear membrane by the histone variant H2A.Z. *J. Cell Biol.* 193:489–507. http://dx.doi.org/10.1083/jcb.201011017

Goedhart, J., D. von Stetten, M. Noirclerc-Savoye, M. Lelimousin, L. Joosen, M.A. Hink, L. van Weeren, T.W. Gadella Jr., and A. Royant. 2012. Structure-guided evolution of cyan fluorescent proteins towards a quantum yield of 93%. *Nat Commun*. 3:751. http://dx.doi.org/10.1038/ncomms1738

Goldberg, M.W., C. Wiese, T.D. Allen, and K.L. Wilson. 1997. Dimples, pores, star-rings, and thin rings on growing nuclear envelopes: evidence for structural intermediates in nuclear pore complex assembly. *J. Cell Sci.* 110:409–420.

Hachet, V., C. Busso, M. Toya, A. Sugimoto, P. Askjaer, and P. Gönczy. 2012. The nucleoporin Nup205/NPP-3 is lost near centrosomes at mitotic onset and can modulate the timing of this process in *Caenorhabditis elegans* embryos. *Mol. Biol. Cell*. 23:3111–3121. http://dx.doi.org/10.1091/mbc.E12-03-0204

Hetzer, M.W., and S.R. Wente. 2009. Border control at the nucleus: biogenesis and organization of the nuclear membrane and pore complexes. *Dev. Cell*. 17:606–616. http://dx.doi.org/10.1016/j.devcel.2009.10.007

Horigome, C., T. Okada, K. Shimazu, S.M. Gasser, and K. Mizuta. 2011. Ribosome biogenesis factors bind a nuclear envelope SUN domain protein to cluster yeast telomeres. *EMBO J.* 30:3799–3811. http://dx.doi.org/10.1038/emboj.2011.267

Jaspersen, S.L., and M. Winey. 2004. The budding yeast spindle pole body: structure, duplication, and function. *Annu. Rev. Cell Dev. Biol.* 20:1–28. http://dx.doi.org/10.1146/annurev.cellbio.20.022003.114106

Jaspersen, S.L., T.H. Giddings Jr., and M. Winey. 2002. Mps3p is a novel component of the yeast spindle pole body that interacts with the yeast centrin homologue Cdc31p. *J. Cell Biol.* 159:945–956. http://dx.doi.org/10.1083/jcb.200208169

Jaspersen, S.L., A.E. Martin, G. Glazko, T.H. Giddings Jr., G. Morgan, A. Mushegian, and M. Winey. 2006. The Sad1-UNC-84 homology domain in Mps3 interacts with Mps2 to connect the spindle pole body with the nuclear envelope. *J. Cell Biol.* 174:665–675. http://dx.doi.org/10.1083/jcb.200601062

Kupke, T., L. Di Cecco, H.M. Müller, A. Neuner, F. Adolf, F. Wieland, W. Nickel, and E. Schiebel. 2011. Targeting of Nbp1 to the inner nuclear membrane is essential for spindle pole body duplication. *EMBO J.* 30:3337–3352. http://dx.doi.org/10.1038/emboj.2011.242

Lau, C.K., T.H. Giddings Jr., and M. Winey. 2004. A novel allele of *Saccharomyces cerevisiae NDC1* reveals a potential role for the spindle

pole body component Ndc1p in nuclear pore assembly. *Eukaryot. Cell*. 3:447–458. http://dx.doi.org/10.1128/EC.3.2.447-458.2004

Lau, C.K., V.A. Delmar, and D.J. Forbes. 2006. Topology of yeast Ndc1p: predictions for the human NDC1/NET3 homologue. *Anat. Rec. A Discov. Mol. Cell. Evol. Biol.* 288:681–694. http://dx.doi.org/10.1002/ar.a.20335

Liu, H.L., C.P. De Souza, A.H. Osmani, and S.A. Osmani. 2009. The three fungal transmembrane nuclear pore complex proteins of *Aspergillus nidulans* are dispensable in the presence of an intact An-Nup84-120 complex. *Mol. Biol. Cell*. 20:616–630. http://dx.doi.org/10.1091/mbc.E08-06-0628

Longtine, M.S., A. McKenzie III, D.J. Demarini, N.G. Shah, A. Wach, A. Brachat, P. Philippsen, and J.R. Pringle. 1998. Additional modules for versatile and economical PCR-based gene deletion and modification in *Saccharomyces cerevisiae*. *Yeast*. 14:953–961. http://dx.doi.org/10.1002/(SICI)1097-0061(199807)14:10<953::AID-YEA293>3.0.CO;2-U

Madrid, A.S., J. Mancuso, W.Z. Cande, and K. Weis. 2006. The role of the integral membrane nucleoporins Ndc1p and Pom152p in nuclear pore complex assembly and function. *J. Cell Biol.* 173:361–371. http://dx.doi.org/10.1083/jcb.200506199

Mansfeld, J., S. Güttinger, L.A. Hawryluk-Gara, N. Panté, M. Mall, V. Galy, U. Haselmann, P. Mühlhäusser, R.W. Wozniak, I.W. Mattaj, et al. 2006. The conserved transmembrane nucleoporin NDC1 is required for nuclear pore complex assembly in vertebrate cells. *Mol. Cell*. 22:93–103. http://dx.doi.org/10.1016/j.molcel.2006.02.015

McCully, E.K., and C.F. Robinow. 1971. Mitosis in the fission yeast *Schizosaccharomyces pombe*: a comparative study with light and electron microscopy. *J. Cell Sci.* 9:475–507.

McDonald, K. 1999. High-pressure freezing for preservation of high resolution fine structure and antigenicity for immunolabeling. *Methods Mol. Biol.* 117:77–97.

Mitchell, J.M., J. Mansfeld, J. Capitanio, U. Kutay, and R.W. Wozniak. 2010. Pom121 links two essential subcomplexes of the nuclear pore complex core to the membrane. *J. Cell Biol.* 191:505–521. http://dx.doi.org/10.1083/jcb.201007098

O'Toole, E.T., M. Winey, and J.R. McIntosh. 1999. High-voltage electron tomography of spindle pole bodies and early mitotic spindles in the yeast *Saccharomyces cerevisiae*. *Mol. Biol. Cell*. 10:2017–2031. http://dx.doi.org/10.1091/mbc.10.6.2017

Onischenko, E., L.H. Stanton, A.S. Madrid, T. Kieselbach, and K. Weis. 2009. Role of the Ndc1 interaction network in yeast nuclear pore complex assembly and maintenance. *J. Cell Biol.* 185:475–491. http://dx.doi.org/10.1083/jcb.200810030

Osmani, A.H., J. Davies, H.L. Liu, A. Nile, and S.A. Osmani. 2006. Systematic deletion and mitotic localization of the nuclear pore complex proteins of *Aspergillus nidulans*. *Mol. Biol. Cell*. 17:4946–4961. http://dx.doi.org/10.1091/mbc.E06-07-0657

Ounjai, P., K.D. Kim, H. Liu, M. Dong, A.N. Tauscher, H.E. Witkowska, and K.H. Downing. 2013. Architectural insights into a ciliary partition. *Curr. Biol.* 23:339–344. http://dx.doi.org/10.1016/j.cub.2013.01.029

Rasala, B.A., C. Ramos, A. Harel, and D.J. Forbes. 2008. Capture of AT-rich chromatin by ELYS recruits POM121 and NDC1 to initiate nuclear pore assembly. *Mol. Biol. Cell*. 19:3982–3996. http://dx.doi.org/10.1091/mbc.E08-01-0012

Ries, J., and P. Schwille. 2006. Studying slow membrane dynamics with continuous wave scanning fluorescence correlation spectroscopy. *Biophys. J.* 91:1915–1924. http://dx.doi.org/10.1529/biophysj.106.082297

Ries, J., S.R. Yu, M. Burkhardt, M. Brand, and P. Schwille. 2009. Modular scanning FCS quantifies receptor-ligand interactions in living multicellular organisms. *Nat. Methods*. 6:643–645. http://dx.doi.org/10.1038/nmeth.1355

Robbins, E., and N.K. Gonatas. 1964. The ultrastructure of a mammalian cell during the mitotic cycle. *J. Cell Biol.* 21:429–463. http://dx.doi.org/10.1083/jcb.21.3.429

Rothballer, A., and U. Kutay. 2013. The diverse functional LINCs of the nuclear envelope to the cytoskeleton and chromatin. *Chromosoma*. 122:415–429. http://dx.doi.org/10.1007/s00412-013-0417-x

Ruan, Q., M.A. Cheng, M. Levi, E. Gratton, and W.W. Mantulin. 2004. Spatial-temporal studies of membrane dynamics: scanning fluorescence correlation spectroscopy (SFCS). *Biophys. J.* 87:1260–1267. http://dx.doi.org/10.1529/biophysj.103.036483

Schwille, P., F.J. Meyer-Almes, and R. Rigler. 1997. Dual-color fluorescence cross-correlation spectroscopy for multicomponent diffusional analysis in solution. *Biophys. J.* 72:1878–1886. http://dx.doi.org/10.1016/S0006-3495(97)78833-7

Sezen, B., M. Seedorf, and E. Schiebel. 2009. The SESA network links duplication of the yeast centrosome with the protein translation machinery. *Genes Dev.* 23:1559–1570. http://dx.doi.org/10.1101/gad.524209

Sheff, M.A., and K.S. Thorn. 2004. Optimized cassettes for fluorescent protein tagging in *Saccharomyces cerevisiae*. *Yeast*. 21:661–670. http://dx.doi.org/10.1002/yea.1130

Shimizu, Y., T. Akashi, A. Okuda, A. Kikuchi, and K. Fukui. 2000. NBP1 (Nap1 binding protein 1), an essential gene for G2/M transition of *Saccharomyces cerevisiae*, encodes a protein of distinct sub-nuclear localization. *Gene*. 246:395–404. http://dx.doi.org/10.1016/S0378-1119(00)00067-6

Sikorski, R.S., and P. Hieter. 1989. A system of shuttle vectors and yeast host strains designed for efficient manipulation of DNA in *Saccharomyces cerevisiae*. *Genetics*. 122:19–27.

Slaughter, B.D., and R. Li. 2010. Toward quantitative "in vivo biochemistry" with fluorescence fluctuation spectroscopy. *Mol. Biol. Cell*. 21:4306–4311. http://dx.doi.org/10.1091/mbc.E10-05-0451

Slaughter, B.D., J.R. Unruh, and R. Li. 2011. Fluorescence fluctuation spectroscopy and imaging methods for examination of dynamic protein interactions in yeast. *Methods Mol. Biol.* 759:283–306. http://dx.doi.org/10.1007/978-1-61779-173-4_17

Snider, J., S. Kittanakom, D. Damjanovic, J. Curak, V. Wong, and I. Stagljar. 2010. Detecting interactions with membrane proteins using a membrane two-hybrid assay in yeast. *Nat. Protoc.* 5:1281–1293. http://dx.doi.org/10.1038/nprot.2010.83

Stafstrom, J.P., and L.A. Staehelin. 1984. Dynamics of the nuclear envelope and of nuclear pore complexes during mitosis in the *Drosophila* embryo. *Eur. J. Cell Biol.* 34:179–189.

Stagljar, I., and S. Fields. 2002. Analysis of membrane protein interactions using yeast-based technologies. *Trends Biochem. Sci.* 27:559–563. http://dx.doi.org/10.1016/S0968-0004(02)02197-7

Starr, D.A., and H.N. Fridolfsson. 2010. Interactions between nuclei and the cytoskeleton are mediated by SUN-KASH nuclear-envelope bridges. *Annu. Rev. Cell Dev. Biol.* 26:421–444. http://dx.doi.org/10.1146/annurev-cellbio-100109-104037

Stavru, F., B.B. Hülsmann, A. Spang, E. Hartmann, V.C. Cordes, and D. Görlich. 2006. NDC1: a crucial membrane-integral nucleoporin of metazoan nuclear pore complexes. *J. Cell Biol.* 173:509–519. http://dx.doi.org/10.1083/jcb.200601001

Strambio-De-Castillia, C., M. Niepel, and M.P. Rout. 2010. The nuclear pore complex: bridging nuclear transport and gene regulation. *Nat. Rev. Mol. Cell Biol.* 11:490–501. http://dx.doi.org/10.1038/nrm2928

Tang, N., and W.F. Marshall. 2012. Centrosome positioning in vertebrate development. *J. Cell Sci.* 125:4951–4961. http://dx.doi.org/10.1242/jcs.038083

Thaminy, S., D. Auerbach, A. Arnoldo, and I. Stagljar. 2003. Identification of novel ErbB3-interacting factors using the split-ubiquitin membrane yeast two-hybrid system. *Genome Res.* 13:1744–1753. http://dx.doi.org/10.1101/gr.1276503

Uetz, P., L. Giot, G. Cagney, T.A. Mansfield, R.S. Judson, J.R. Knight, D. Lockshon, V. Narayan, M. Srinivasan, P. Pochart, et al. 2000. A comprehensive analysis of protein-protein interactions in *Saccharomyces cerevisiae*. *Nature*. 403:623–627. http://dx.doi.org/10.1038/35001009

West, R.R., E.V. Vaisberg, R. Ding, P. Nurse, and J.R. McIntosh. 1998. cut11(+): A gene required for cell cycle-dependent spindle pole body anchoring in the nuclear envelope and bipolar spindle formation in *Schizosaccharomyces pombe*. *Mol. Biol. Cell*. 9:2839–2855. http://dx.doi.org/10.1091/mbc.9.10.2839

Winey, M., and K. Bloom. 2012. Mitotic spindle form and function. *Genetics*. 190:1197–1224. http://dx.doi.org/10.1534/genetics.111.128710

Winey, M., M.A. Hoyt, C. Chan, L. Goetsch, D. Botstein, and B. Byers. 1993. NDC1: a nuclear periphery component required for yeast spindle pole body duplication. *J. Cell Biol.* 122:743–751. http://dx.doi.org/10.1083/jcb.122.4.743

Witkin, K.L., J.M. Friederichs, O. Cohen-Fix, and S.L. Jaspersen. 2010. Changes in the nuclear envelope environment affect spindle pole body duplication in *Saccharomyces cerevisiae*. *Genetics*. 186:867–883. http://dx.doi.org/10.1534/genetics.110.119149